Research Square

Preprints are preliminary reports that have not undergone peer review.
They should not be considered conclusive, used to inform clinical practice,
or referenced by the media as validated information.

Modeling and Multiple Fractional Solutions for Two-Phase Blood Flow in a Slant Cylindrical Tube with Memory Effect

Maher Jebali
University of Ha'il
Muhammad Saqib
muhammadsaqib621@gmail.com
Qurtuba University of Science and Information Technology
Zeineb Klai
Northern Border University
Mohamed Bouzidi
University of Ha'il

Article

Keywords: Blood flow, Magnetic Particles, Magnetohydrodynamic, Fractional Calculus, Integral Transforms

Posted Date: October 20th, 2025

DOI: https://doi.org/10.21203/rs.3.rs-7677402/v1

License: This work is licensed under a Creative Commons Attribution 4.0 International License.
Read Full License

Additional Declarations: No competing interests reported.

Modeling and Multiple Fractional Solutions for Two-Phase Blood Flow in a Slant Cylindrical Tube with Memory Effect

Maher Jebali[1], Muhammad Saqib[2,*], Zeineb Klai[3,*], Mohamed Bouzidi[4]

[1]Computer Science Department, Applied College, University of Ha'il, P.O. Box 2440, Hail City, 55476, Saudi Arabia.

[2]Department of Physical and Numerical Sciences, Qurtuba University of Science and Information Technology, Peshawar 25100, KP, Pakistan

[3]Department of Computer Sciences Faculty of Computing and Information Technology Northern Border University Kingdom of Saudi Arabia.

[4]Department of Physics, College of Science, University of Ha'il, P.O. Box 2440, Ha'il, Saudi Arabia.

Abstract: This work investigates the magnetohydrodynamic (MHD) flow of blood in an inclined cylindrical tube containing infused magnetic nanoparticles (MNPs). This system has significant implications for hyperthermia treatment and targeted drug administration. It is crucial for comprehending completely the interdependent effects of MNPs, tube inclination, and MHD. The Brinkman type fluid model is employed in the established two-phase flow. The Caputo, Caputo-Fabrizio (CF), and Atangana-Baleanu (AB) fractional operators are used in succeeding fractionalization to account for memory effects and allow for a comparison analysis between various fractional frameworks. The joint Laplace-Hankel transforms are used to produce the exact solutions. When $\alpha \to 1$ the classical results are restored. The results reveal that velocities caused by Lorentz forces decrease as the magnetic number (M) increases, with CF showing the fastest reaction. At the same time, because of stronger viscous and inertial effects, higher particle concentrations (P_C) reduce velocities. The fractional orders ($\alpha, \beta, \text{and } \gamma$), display dual time-dependent dynamics, speeding up flows over extended periods ($t = 1.5$ after initially slowing them down. The most physically accurate predictions are produced by AB's Mittag-Leffler kernel, which combines short- and long-term memory effects. The results show the importance of fractional calculus in simulating complex biofluid dynamics, particularly in inclined tubes where gravity, magnetic, and viscous forces interact, and they offer a solid foundation for enhancing magnetic drug delivery devices.

Keywords: *Blood flow; Magnetic Particles; Magnetohydrodynamic; Fractional Calculus; Integral Transforms*

**Corresponding Authors: muhammadsaqib621@gmail.com (Muhammad Saqib) and Zeineb.klai@nbu.edu.sa (Zeineb Klai)*

1. Introduction

The study of blood flow under the action of magnetic fields has gained a lot of interest, as it may lead to important applications in medical technology (e.g. targeted drug delivery). Blood is one of

the fluids that contains hemoglobin rich in iron and therefore got magnetized. Studies of human blood show that it has distinct behavior depending on whether the blood is oxygenated or not. If it is oxygenated, behave as diamagnetic and if it is deoxygenated acts as paramagnetic. Investigations reveal that this can be influenced by applying external magnetic fields reducing its flow by up to 30%.[1, 2]. The understanding of the interaction of blood flow and magnetic fields is of interest for the development of biomedical tracers (magnetic tracers) as well as targeted drug delivery. Yet most classical models of blood flow assume that blood is a simple Newtonian fluid that is non-conducting which is inaccurate as blood plasma contains ions and conducts electricity. Because of this, the flow is impacted by both magnetic nanoparticles particles (MNPs) and magnetohydrodynamic (MHD), therefore an individual model excluding one of these effects is incomplete. Some recent studies have attempted to improve this by making two phase mathematical models capture the properties of both magnetic particles and MHD. For instance, Murtaza *et al.* [3] discussed the combination of both MNPs and MHD blood flow over a stretching sheet. Their research, reveal that using both MNPs and MHD play an significant role, as they make an noticeable and computable difference in the flow.

In addition, Javeed and Jung [4] used a two-phased model to investigate how MHD affected blood flow. By building a numerical algorithm to replicate the blood flow model, they produced numerical findings. They were able to precisely investigate the blood flow pattern impacted by changes in artery diameter and magnetic field strength thanks to this technique. Chrimatopoulos *et al.* [5] used the finite volume approach to computationally study nonlinear equations describing MHD blood flow with MNPs. They showed how magnetic fields caused by Lorentz forces reduced the blood's flow rate. A significant explanation of non-isothermal MHD models using MNPs was carried out by Könözsy *et al.* [6] who clarified their significant relationship to bio-fluid dynamics (BFD). Their research provides important validation standards for non-Newtonian and non-isothermal blood flow scenarios. They also make the case for the application of these sophisticated models to the improvement of magnetic resonance imaging (MRI) technology and predicting accuracy. In a rectangular channel, MHD blood flow was examined by Kasiman *et al.* [7] They employed the finite volume approach for the simulation. It was discovered that variations skin friction cause variations in blood speed in the model with different magnetic field intensities. According to their models, a higher magnetic field slows down fluid flow and is inversely proportionate to friction on the channel walls. Through numerical simulations and modeling of

MHD blood flow, Rajashekhar *et al.* [8] demonstrated the option of more accurate targeted drug delivery. The results clearly show that it is possible to increase treatment accuracy in blood vessels using magnetic particles. Fenech and Haya [9] examined the influence of MHD on blood flow in arteries. Their research showed that the magnetic forces have a substantial effect on the stress on the walls of the artery as well as the overall flow. The research work was further advanced by Gregory *et al.* [10], and Drochon *et al.* [11] by discussing the dynamic of MNPs and MHD blood. It was demonstrated that distinct blood flow patterns are produced by the interaction effects of MNPs and MHD. The effectiveness of magnetic hyperthermia treatment is improved by certain flow patterns. Although it is exciting to emphasize MNPs and MHD in blood flow modeling, it seems to allow critical phase since blood is a type of fluid that can be accurately described by fractional calculus approaches and is non-Newtonian with memory effect.

Recent advancements in fractional calculus offer a reliable mathematical model for simulating intricate biological fluids like blood.These approaches have the potential of integrating memory effects with the underlying hereditary characteristics, which has been shown to be a weak point for the classical integer order models [12-14]. Fractional derivative operators such as Caputo [15], CF [16], and AB [17] definitions are used in most of the biofluid dynamics applications [18-20]. They are able to describe anomalous and viscoelasticity which cannot be well simulated with purely ordinary calculus. With its single kernel, the Caputo fractional operator is frequently employed because it works well with common boundary conditions. This is followed by the CF fractional derivative using a non-singular exponential kernel. This eliminates singularities and makes it easier for the model to depict rapid changes. [21-23]. A more general mathematical foundation is provided by the construction of the AB fractional derivative operator, which uses the Mittag-Leffler function as its kernel. Because it takes into account the impacts of both short-term and long-term memory, this method is appropriate for modeling biological systems with a wide range of behavioral dimensions [24, 25].

Significant insights into the dynamics of blood MNPs interactions under various physiological situations can be gained by analyzing magnetic blood flow using the Caputo, CF, and AB fractional derivatives operators. Using the CF fractional derivative model, Riaz and Zafar [26] were able to successfully investigate blood flow in cylindrical tubes under the influence of a magnetic field. According to their research, the CF technique accurately interprets the influence of physical

parameters on velocity field, making it a robust framework for blood flow modeling. Saikia *et al.* [27, 28] investigated MHD flow across vertical surfaces using the AB fractional derivative operator. The crucial differences in viscosity and thermal conductivity that are seen in biological fluids like blood were integrated in their model. Their findings show that the intricate relationship between heat radiation and viscous dissipation is captured by the AB fractional derivative. The comprehension of heat and mass transmission is enhanced by this expressive ability. The CF and AB approaches produce comparable results for temperature and velocity profiles. This implies that for the predictive modeling of magnetic blood flows, each fractional operator is equally viable [29].

Fractional-order derivative models have seen an increase in interest in recent fluid dynamics research. These models provide greater potential for non-local memory effects and exhibited sophisticated substantial behaviors, which are frequently incompetently covered by traditional integer-order approaches. Non-local kernels, which provide an extra physically realistic representation of real-world occurrences, are introduced via their employment. As a result, they have been successfully used in a variety of fields, including biofluid mechanics and quantum physics [30]. This advancement in mathematics has opened up completely new possibilities for simulating intricate biological structures. In hemodynamics, where accurate representation of anomalous diffusion and genetic memory effects is crucial, it is primarily transformative. Through the development of analytical solutions for MHD blood flow inside static cylindrical tubes, Ali *et al.* [31] enhanced the use of fractional derivatives in hemodynamics. This study was then expanded to include the impact of oscillating boundaries on cylindrical geometry [32] demonstrating the high degree of compliance of fractional calculus methods with a wide variety of intricate boundary conditions. Porosity factors were incorporated into fractional MHD blood flow models by Maiti *et al.* [33], who subsequently advanced the field of study. In a parallel advancement, Jamil *et al.* [34] proceed forward the research by considering the inclination in flow geometry. Both studies utilized a fractional derivative approche, obtaining analytical solutions hybrid methodologies that integrate Laplace finite Hankel transforms, thus, developing a strong mathematical methodology for fractional hemodynamic modeling.

Previous studies have widely examined hemodynamic models utilizing either classical integer-order derivatives or singular fractional operator methodologies. However, a comparative

investigation combing multiple fractional operators such as Caputo, CF and AB fractional operators within a combined framework for blood flow has not been investigated in the open literature. This gap presents a substantial opportunity for advancing this field. Therefore, the primary objective of the study is to close this important gap by conducting a thorough fractional examination of two-phase blood flow in an inclined cylindrical tube with uniformly loaded MNPs. For this purpose, the Brinkman-type fluid model in terms of Caputo, CF, and AB fractional derivative operators are being used in this study. This approach improves the research capacity of hemodynamic modeling in complicated geometry by allowing the study of memory effects and non-local dynamics. Joint Laplace and Hankel transformations are used in this study to provide exact solutions. Results from three different fractional operators, including Caputo, CF, and AB, are compared and shown. The impact of important parameters, such as fractional order, magnetic, particle concentration, and the Brinkman parameters, is examined in this work. These studies clarify how each parameter affects the velocities of blood and MNPs. The results offer important insights for improving magnetic drug delivery. Additionally, they offer a theoretical foundation for further experimental research in this field. In the framework of blood flow modeling with magnetic particles (MPs), the present paper is the first study to compare of several fractional operators.

2. Mathematical Formulation

Let us examine the blood flow in which MPs are homogeneously dispersed within a cylindrical vessel of radius of r_0 as illustrated in Figure 1. The slant-oriented cylindrical vessel is made an inclination angle θ along the z-axis, while the r-axis is perpendicular to this orientation. The blood and the MP are flowing along this direction, while an inclined magnetic field of specified intensity B_0 is exerting its influence upon them. The magnetic Reynold number is assumed to be small, neglecting the induced magnetic field. At $t \le 0$, the blood, MPs and tube remain at rest. But, at $t = 0^+$ the blood and MPs start motion in the z-direction with an angle θ due to the pressure gradient. For the two-phase blood flow, the governing equations based on the Brinkman-type fluid model required an extra term referred to as force interaction among blood and MPs. Thus, refer to Rajagopal [35], Fetecau [36], Saffman [37], Marble[38] and Ali *et al.* [31] the governing equations are as follow

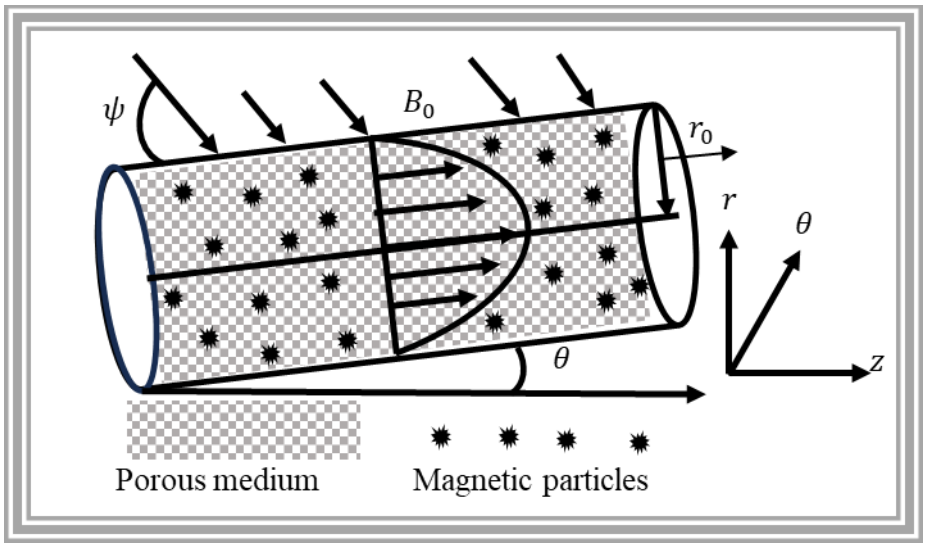


Figure 1: Physical geometry of the flow

$$\nabla.\mathbf{V} = 0\,, \tag{1}$$

$$\rho\frac{d\mathbf{V}}{dt} = \nabla.\underline{\mathbf{T}} - \alpha_d\mathbf{V} + \mathbf{F_b} + \mathbf{F_p} + \rho\mathbf{g}\,, \tag{2}$$

$$m_p\frac{\partial u_{pz}(r,t)}{\partial t} = K\left\{u_z(r,t) - u_{pz}(r,t)\right\}, \tag{3}$$

where ρ is the density of blood, d/dt is the material time derivative, $\underline{\mathbf{T}}$ is the Cauchy stress tensor, α_d is the positive coefficient of drag force of porous medium, $\mathbf{F_b}$ is the body force and $\mathbf{F_p}$ is the total fluid-particle interaction force per unit volume, m_p is the average mass of MPs and $u_{p_z}(r,t)$ is the velocity of MPs. Assuming the velocity field of the form $\mathbf{V} = \{0,0,u_z(r,t)\}$ then term $\frac{d\mathbf{V}}{dt}$ and $\nabla.\underline{\mathbf{T}}$ reduced to the following form

$$\frac{D\mathbf{V}}{Dt} = \left(\frac{\partial u_z(r,t)}{\partial t}\right)\mathbf{e}_z\,, \tag{4}$$

$$\nabla.\underline{\mathbf{T}} = -\frac{\partial p}{\partial z} + \mu\left(\frac{\partial^2 u_z}{\partial r^2} + \frac{1}{r}\frac{\partial u_z}{\partial r}\right). \tag{5}$$

Using Maxwell's set of equations, the body forces $\mathbf{F_b}$ is given by

$$\mathbf{F} = \mathbf{J} \times \mathbf{B} = \sigma_0[\mathbf{E} + \mathbf{V} \times \mathbf{B}] \times \mathbf{B} = -\sigma B_0^2 u(r,t)\vec{k} \sin^2 \psi \,. \tag{6}$$

As in the case of two-phase blood flow, there is a force of interaction between the blood and the MPs. So, it is necessary to formulate the blood and MPs equations of motion independently. When the Reynold number is less than unity and depends on the relative particle velocity, the force that accelerates the particles to the fluid speed can be written as $6\pi\mu r_p\left(\mathbf{V}_p - \mathbf{V}\right)$. This is known as Stokes law, where r_p is the particle's radius and μ is the dynamic viscosity. Next, the total force of interaction per unit volume is determined by [39, 40]

$$\mathbf{F_p} = n6\pi\mu r_p\left(u_{pz} - u_z\right), \tag{7}$$

equivalently

$$\mathbf{F_p} = \frac{\rho_p}{\tau_v}\left(u_{pz} - u_z\right), \tag{8}$$

where ρ_p is the density of MPs and τ_v is relaxation time for the MPs change then, keeping in view $\mathbf{V} = \left\{0, 0, u_z(r,t)\right\}$ and incorporating Eqs. (4)-(7), (8) into Eq. (2) yield to

$$\begin{aligned}\rho\frac{\partial u_z(r,t)}{\partial t} = &-\frac{\partial p}{\partial z} + \mu\left(\frac{\partial^2 u_z(r,t)}{\partial r^2} + \frac{1}{r}\frac{\partial u_z(r,t)}{\partial r}\right) - \alpha_d u_z(r,t) - \sigma B_0^2 u_z(r,t)\sin\psi \\ &+ \frac{\rho_p}{\tau_v}\left\{u_{pz}(r,t) - u_z(r,t)\right\} + \rho g \sin\theta.\end{aligned} \tag{9}$$

Equivalently

$$\begin{aligned}\rho\left(\frac{\partial u_z(r,t)}{\partial t} + \beta_d u_z(r,t)\right) = &-\frac{\partial p}{\partial z} + \mu\left(\frac{\partial^2 u_z(r,t)}{\partial r^2} + \frac{1}{r}\frac{\partial u_z(r,t)}{\partial r}\right) - \sigma B_0^2 u_z(r,t)\sin\psi \\ &+ KN\left\{u_{pz}(r,t) - u_z(r,t)\right\} + \rho g \sin\theta,\end{aligned} \tag{10}$$

where $\beta_b = \alpha_d / \rho$ is the Brinkman-type fluid parameter, K is the Stocks' constant, and N is the number of MPs per unit volume. The pressure gradient $\frac{\partial p}{\partial z}$ is taken of oscillating form as [41]

$$\frac{\partial p}{\partial z} = -\lambda_0 - \lambda_1 \cos(\omega t), \tag{11}$$

where λ_0 and λ_1 are the amplitudes of pressure gradient that give rise to systolic or diastolic pressure. Substituting Eq. (11) into Eq. (10) yields to

$$\begin{aligned}\rho\left(\frac{\partial u_z(r,t)}{\partial t} + \beta_d u_z(r,t)\right) &= \lambda_0 + \lambda_1 \cos(\omega t) + \mu\left(\frac{\partial^2 u_z(r,t)}{\partial r^2} + \frac{1}{r}\frac{\partial u_z(r,t)}{\partial r}\right) \\ &+ KN\left\{u_{pz}(r,t) - u_z(r,t)\right\} - \sigma {B_0}^2 u_z(r,t) + \rho g \sin\theta.\end{aligned} \tag{12}$$

The governing equations, Eqs. (3),(12) related to the flow configuration, are constrained by the following relevant initial and boundary conditions

$$u_z(r,0) = 0,\ u_{pz}(r,0) = 0, \tag{13}$$

$$u_z(r_0,t) = 0, u_{pz}(r_0,\mathrm{t}) = 0, \left.\frac{\partial u_z(r,t)}{\partial r}\right|_{r=0} = 0\Bigg\}. \tag{14}$$

3. Development of Fractional Models

Introducing the following dimensionless variable

$$f = \frac{u_z}{u_0}, g = \frac{u_{pz}}{u_0}, t^* = \frac{t\nu}{{r_0}^2}, r^* = \frac{r}{r_0}, \phi_0 = \frac{r_0^2}{u_0\mu}\lambda_0,\ \phi_1 = \frac{r_0^2}{u_0\mu}\lambda_1,$$

into Eq. (3) and Eq. (12)-(14) and dropping the * sign for simplicity yield to

$$\begin{aligned}\frac{\partial f(r,t)}{\partial t} &= \phi_0 + \phi_1 \cos\omega t + \frac{\partial^2 f(r,t)}{\partial r^2} + \frac{1}{r}\frac{\partial f(r,t)}{\partial r} \\ &+ P_C\left\{g(r,t) - f(r_1,\tau)\right\} - M_0 u(r,t)\sin\psi + \Omega\sin\theta\end{aligned}, \tag{15}$$

$$P_m \frac{\partial g(r,t)}{\partial t} = f(r,t) - g(r,t), \tag{16}$$

along with

$$f(r,0) = 0,\ g(r,0) = 0, \tag{17}$$

$$f(1,t) = 0,\ g(1,t) = 0, \left. \frac{\partial f(r,1)}{\partial r} \right|_{r=0} = 0 \Bigg\}, \tag{18}$$

where $\beta_1 = \frac{r_0^2 \beta_d}{\upsilon}$ is the Brinkman parameter, $P_C = \frac{r_0{}^2 KN}{\mu}$ is the particle concentration parameter, $P_m = \frac{m\upsilon}{r_0{}^2 K}$ is the particle mass parameter and $M = \frac{r_0{}^2 \sigma B^2{}_0}{\mu}$ is the magnetic parameter and $\Omega = \frac{r_0^2}{u_0 \upsilon}$, $M_0 = M \sin\psi - \beta_1$ are constant terms. To develop generalized fractional models, time derivative in Eqs. (15) and (16) are replaced with Caputo, CF, and AB fractional operators which yield the following multiple fractional models.

3.1 Caputo Time Fractional Model

The Caputo fractional derivative is using a singular power-law kernel and offers a theoretically straightforward framework for describing memory-dependent phenomena while preserving compatibility with conventional initial conditions. Its benefit is in its simple Laplace transform representation, which streamlines the analytical handling of fractional differential equations. We generalize the governing equations to include non-local temporal effects in blood flow dynamics by incorporating the Caputo time-fractional derivative into Eqs. (15) and (16) yield to

$$\begin{aligned} {}^{C}D_t^{\alpha} f_C(r,t) = {} & \phi_0 + \phi_1 \cos\omega t + \frac{\partial^2 f_C(r,t)}{\partial r^2} + \frac{1}{r}\frac{\partial f_C(r,t)}{\partial r} + P_C \left\{ g_C(r,t) - f_C(r,t) \right\} \\ & - M_0 f_C(r,y) \sin\psi + \Omega \sin\theta \end{aligned} \tag{19}$$

$$P_m {}^{C}D_t^{\alpha} g_C(r,t) = f_C(r,t) - g_C(r,t), \tag{20}$$

subject to

$$f_C(r,0)=0,\ g_C(r,0)=0, \tag{21}$$

$$f_C(1,t)=0,\ g_C(1,t)=0,\left.\frac{\partial f_C(r,1)}{\partial r}\right|_{r=0}=0\Bigg\}, \tag{22}$$

where ${}^{C}D_t^{\alpha}(.,.)$ is the Caputo fractional operator and is given by [15]

$$D_t^{\alpha}h(\eta,\mathrm{t})=\begin{cases}\dfrac{1}{\Gamma(1-\alpha)}\displaystyle\int_0^t\frac{1}{(t-s)^{\alpha}}\frac{\partial h(\eta,s)}{\partial s}ds;0<\alpha<1\\ \dfrac{\partial h(\eta,\mathrm{t})}{\partial t};\alpha=1\end{cases} \tag{23}$$

The above-altered model allows a more accurate description of the time-dependent behavior of the flow by accounting for the genetic characteristics of blood viscosity and particle-fluid interactions. This fractional formulation adds memory effects essential for describing complicated biofluid transport events while maintaining the physical interpretation of initial conditions

3.2 CF Time Fractional Model

The CF fractional derivative enhances the representation of rapid transient responses in physical systems by employing a non-singular exponential kernel that circumvents mathematical singularities. In contrast to the power-law kernel of the Caputo derivative, the exponential decay of the CF operator provides gentler memory effects, rendering it particularly suitable for simulating biological flows characterized by rapid relaxation processes. Integrating the CF time-fractional derivative into Eqs. (15) and (16) yield the following generalized model that more accurately represents the short-term dynamics of blood flow and MPs interactions.

$$\begin{aligned}{}^{CF}D_t^{\beta}f_{CF}(r,t)&=\phi_0+\phi_1\cos\omega t+\frac{\partial^2 f_{CF}(r,t)}{\partial r^2}+\frac{1}{r}\frac{\partial f_{CF}(r,t)}{\partial r}\\ &+P_C\left\{g_{CF}(r,t)-f_{CF}(r,t)\right\}\ -M_0 f_{CF}(r,t)\sin\psi+\Omega\sin\theta,\end{aligned} \tag{24}$$

$$P_m\,{}^{CF}D_t^{\beta}g_{CF}(r,t)=f_{CF}(r,t)-g_{CF}(r,t), \tag{25}$$

subject to

$$f_{CF}(r,0)=0,\ g_{CF}(r,0)=0, \tag{26}$$

$$f_{CF}(1,t)=0,\ g_{CF}(1,t)=0,\left.\frac{\partial f_{CF}(r,1)}{\partial r}\right|_{r=0}=0\Bigg\},\tag{27}$$

where ${}^{CF}D_t^{\beta}(.)$ is the CF time fractional operator and is given by [16]

$${}^{CF}D_t^{\beta}h(\eta,t)=\frac{N(\beta)}{1-\beta}\int_0^t\exp\left(-\frac{\beta(t-s)}{1-\beta}\right)\frac{\partial h(\eta,t)}{\partial s}ds;\ 0<\beta<1,,\tag{28}$$

which is the convolution product of the function $\frac{N(\beta)}{1-\beta}\exp\left(-\frac{\beta t}{1-\beta}\right)$ and $\frac{\partial h(\eta,t)}{\partial t}$ of fractional order β and $N(1)=N(0)=1$.

This approach is especially advantageous for articulating the initial acceleration phases and swift stabilization observed in hemodynamic systems. The Laplace transform properties of the CF operator maintain compatibility with physiological initial conditions while facilitating analytical solutions.

3.3 Atangana-Baleanu Time Fractional Model

The AB fractional derivative employs a sophisticated Mittag-Leffler kernel that integrates the advantages of power-law and exponential decay characteristics. This non-singular operator, unlike traditional fractional derivatives, more accurately represents long-range temporal relationships and short-term memory effects. The incorporation of the AB time-fractional derivative in Eqs. (15) and (16) facilitate the development of a comprehensive model that more precisely represents the multi-scale dynamics of blood flow including MPs. The generalized model in terms of AB operator is given by

$$\begin{aligned}&{}^{AB}D_t^{\gamma}f_{AB}(r,t)=\phi_0+\phi_1\cos\omega t+\frac{\partial^2 f_{AB}(r,t)}{\partial r^2}+\frac{1}{r}\frac{\partial f_{AB}(r,t)}{\partial r}\\&+P_C\left\{g_{AB}(r,t)-f_{AB}(r,t)\right\}-M_0 f_{AB}(r,t)\sin\psi+\Omega\sin\theta\end{aligned},\tag{29}$$

$$P_m\,{}^{AB}D_t^{\gamma}g_{AB}(r,t)=f_{AB}(r,t)-g_{AB}(r,t)\ ,\tag{30}$$

subject to

$$f_{AB}(r,0)=0,\ g_{AB}(r,0)=0\,, \tag{31}$$

$$f_{AB}(1,t)=0, g_{AB}(1,t)=0, \left.\frac{\partial f_{AB}(r,t)}{\partial r}\right|_{r=0}=0\Bigg\}, \tag{32}$$

where ${}^{AC}D_{\tau}^{\gamma}(.)$ is the Atangana-Baleanu time fractional derivative operator and is given by [17]

$$D_t^{\gamma}h(\eta,t)=\frac{N(\gamma)}{1-\gamma}\int_0^t E_{\gamma}\left\{\frac{-\gamma(t-s)^{\gamma}}{1-\gamma}\right\}\frac{\partial h(\eta,s)}{\partial s}ds. \tag{33}$$

where $N(\alpha)$ is the normalization function such that $N(1)=N(0)=1$ and $E_{\gamma}(.)$ is the Mittag-Leffler function and is given by [42]

$$E_{\gamma}\left(-t^{\gamma}\right)=\sum_{K=0}^{\infty}\frac{(-t)^{\gamma K}}{\Gamma(\gamma K+1)} \tag{34}$$

The versatility of the Mittag-Leffler kernel enables the simultaneous replication of rapid initial responses and prolonged memory effects observed in complex biological systems. This method is particularly effective for illustrating the intricate interplay between blood rheology and magnetic particle movements over different time scales. The mathematical properties of the AB operator facilitate rapid numerical implementation while maintaining a clear physical understanding of the system's behavior.

4. Solutions to the problem

This section provides exact solutions for the coupled system of fractional PDEs that govern magnetic blood flow, primarily focusing on the Eqs. (19)-(22), (24)-(27), and (29)-(32) with their respective initial and boundary conditions. The solutions are obtained by sophisticated mathematical methods to address the complexities introduced by three different fractional operators: Caputo, CF, and AB. *Solution in terms of*

4.1. Caputo time fractional operator

Using the Laplace transform ($L\left\{f(r,t)\right\}(q)=\bar{f}(q)=\int_0^{\infty}f(r,t)e^{-qt}dt,$) on Eqs. (19) and (20) with initial condition (21) results in the following transformed equations:

$$\frac{d^2\bar{f}_C(r,q)}{\partial r^2}+\frac{1}{r}\frac{d\bar{f}(r,q)}{\partial r}=\left[\frac{P_m q^{2\alpha}+\left\{1+P_m\left(P_C+M_0\right)\right\}q^{\alpha}+M_0}{P_m q^{\alpha}+1}\right]f_C(r,q)-\frac{\phi_2}{q}-\frac{q\phi_1}{q^2+\omega^2}, \tag{35}$$

$$\bar{g}_C\left(r_1,q\right)=\frac{\bar{f}_C\left(r,q\right)}{P_m q^{\alpha}+1}, \tag{36}$$

This transformation reduces the original fractional PDEs to linear ODEs, hence enabling their exact solutions. The procedure maintains all physical parameters while shifting the temporal complexity to the frequency domain. The transformed boundary conditions are as follows

$$\bar{f}_C\left(1,q\right)=0, \left.\frac{\partial f_C\left(1,q\right)}{\partial r}\right|_{r=0}=0,\ \bar{g}_C\left(1,q\right)=0, \tag{37}$$

where $\phi_2=\phi_0+\Omega\sin\theta$.

Using the finite Hankel transform ($H\left\{\bar{f}\left(r,q\right)\right\}\left(r_n\right)=\bar{f}_H\left(r_n,q\right)=\int_0^1 r\bar{f}\left(r,q\right)J_0\left(rr_n\right)dr$) on Eqs. (35)-(36) and including boundary condition (37) yields the following transformed system

$$\bar{f}_{CH}\left(r_n,q\right)=\left[\begin{array}{l}\dfrac{\phi_2}{d_{n2}}\left\{\left(1-P_m d_{n4}\right)\dfrac{q^{-1}}{q^{\alpha}+d_{n4}}-\left(1-P_m d_{n3}\right)\dfrac{q^{-1}}{q^{\alpha}+d_{n3}}\right\}\\ +\dfrac{\phi_1}{d_{n2}}\dfrac{q}{q^2+\omega^2}\left\{\left(1-P_m d_{n4}\right)\dfrac{1}{q^{\alpha}+d_{n4}}-\left(1-P_m d_{n3}\right)\dfrac{1}{q^{\alpha}+d_{n3}}\right\}\end{array}\right]\frac{J_1\left(r_n\right)}{r_n}, \tag{38}$$

and

$$\bar{g}_{CH}\left(r_n,q\right)=\frac{1}{P_m}\left(\frac{1}{q^{\alpha}+\dfrac{1}{P_m}}\right)\bar{f}_{CH}\left(r_n,q\right). \tag{39}$$

where

$$d_{n1}=\left\{1+P_m\left(P_C+M_0\right)+{r_{1n}}^2P_m\right\},\ d_{n2}=\sqrt{\left(d_{1n}\right)^2-4P_m\left({r_{1n}}^2+M_0\right)},\ d_{n3}=\frac{d_{n1}+d_{n2}}{2P_m}, d_{n4}=\frac{d_{n1}-d_{n2}}{2P_m}.$$

This process transforms spatial derivatives into algebraic expressions, thereby simplifying the ODEs to a more manageable form while preserving the essential features of cylindrical geometry. The boundary condition (37) guarantees that appropriate physical constraints are maintained

throughout this transformation. Applying the inverse Laplace transform to Eqs. (38) and (39) yield to

$$g_{CH}\left(r_n,t\right)=\frac{1}{P_m}\left\{F_\alpha\left(-\frac{1}{P_m},t\right)*f_{CH}\left(r_{1n},t\right)\right\}, \tag{40}$$

$$f_{CH}\left(r_n,t\right)=X\left(t\right)\frac{J_1\left(r_n\right)}{r_n}+Y\left(t\right)\frac{J_1\left(r_n\right)}{r_n}, \tag{41}$$

where

$$X\left(t\right)=\frac{\phi_2}{d_{n2}}\left\{\left(1-P_m d_{4n}\right)R_{\alpha,-1}\left(-d_{n4},t\right)-\left(1-P_m d_{n3}\right)R_{\alpha,-1}\left(-d_{n3},t\right)\right\} \tag{42}$$

$$Y\left(t\right)=\frac{\phi_1}{d_{2n}}\cos\omega t*\left\{\left(1-P_m d_{4n}\right)F_{\alpha,-1}\left(-d_{n4},t\right)-\left(1-P_m d_{n3}\right)F_{\alpha,-1}\left(-d_{n3},t\right)\right\}. \tag{43}$$

In Eqs. (40) and (41), the * sign represents the convolution product. The $R_{\alpha,-1}\left(-d_{n4},\tau\right)$ and $F_{\alpha,-1}\left(-d_{n4},\tau\right)$ are respectively Lorenzo and Hartleys' and Robotnov and Hartleys' functions and are given by [31]

$$R_{\alpha,\upsilon}\left(-\xi,t\right)=\sum_{k=0}^{\infty}\frac{\left(-\xi\right)^k t^{(k+1)\alpha-1-\upsilon}}{\Gamma\left\{\left(k+1\right)\alpha-\upsilon\right\}}=L^{-1}\left\{\frac{q^{-\upsilon}}{q^\alpha+\xi}\right\} \tag{44}$$

$$F_\alpha\left(-\xi,t\right)=\sum_{k=0}^{\infty}\frac{\left(-\xi\right)^k t^{(k+1)\alpha-1}}{\Gamma\left\{\left(k+1\right)\alpha\right\}}=L^{-1}\left\{\frac{1}{q^\alpha+\xi}\right\}. \tag{45}$$

Following the Hankel transform inversion, we obtained the exact solutions in the physical domain, which are as follows:

$$g_C\left(r,\tau\right)=\frac{1}{P_m}\int_0^\tau F_\alpha\left(-\frac{1}{P_m},s\right)f_C\left(r,\tau-s\right)ds, \tag{46}$$

$$f_C\left(r,\tau\right)=2\sum_{n=1}^{\infty}\frac{J_0\left(r_1 r_{1n}\right)}{r_{1n}J_1\left(r_{1n}\right)}\left\{X\left(\tau\right)+Y\left(\tau\right)\right\}. \tag{47}$$

Maintaining all physical parameters and boundary effects, this inversion method reconstructs the whole spatial solution from its Hankel-transformed components, restoring the radial dependency of the velocity and particle distribution profiles. Though entirely resolved in both spatial and temporal dimensions, the resulting expressions maintain the cylindrical symmetry of the original problem.

4.2 Solution in terms of CF fractional operator

The CF time fractional derivatives and Eqs. (24) and (25) are transformed using the Laplace transform method using initial conditions (26) and boundary conditions (27) to produce:

$$\frac{q}{(1-\beta)q+\beta}\bar{f}_{CF}(r,q)=\frac{\phi_2}{q}+\frac{\phi_1 q}{q^2+\omega^2}+\frac{d^2\bar{f}_{CF}(r,q)}{\partial r^2}+\frac{1}{r}\frac{\partial\bar{f}_{CF}(r,q)}{\partial r}$$
$$+P_C\left\{\bar{g}_{CF}(r,q)-\bar{f}_{CF}(r,q)\right\}-M_0\sin\psi\,\bar{f}_{CF}(r,q), \tag{48}$$

$$\bar{g}_{CF}(r,q)=\left\{\frac{(1-\beta)q+\beta}{P_m q+(1-\beta)q+\beta}\right\}\bar{f}(r,q). \tag{49}$$

and

$$\bar{f}_{CF}(1,q)=0,\ \bar{g}_{CF}(1,q)=0,\frac{\partial\bar{f}_{CF}(r,q)}{\partial r}\bigg|_{r=0}=0\Bigg\}, \tag{50}$$

This transformation preserves the non-singular character of the solutions and simplifies the fractional terms using the exponential kernel characteristics of the CF operator. The initial and boundary conditions guarantee physical consistency all over the transformation process, therefore producing analytically tractable equations in the Laplace domain. Next, Eq. (49) is used in Eq. (48) and after simplification, we arrived at:

$$\left\{\frac{\chi_a(\beta)q^2+\chi_b(\beta)q+\chi_c(\beta)}{\chi_d(\beta)q^2+\chi_e(\beta)q+\beta^2}\right\}\bar{f}_{CF}(r,q)=\frac{\phi_2}{q}+\frac{\phi_1 q}{q^2+\omega^2}+\frac{d^2\bar{f}_{CF}(r,q)}{\partial r^2}+\frac{1}{r}\frac{\partial\bar{f}_{CF}(r,q)}{\partial r}, \tag{51}$$

where

$$\chi_a(\beta)=P_m+(1-\beta)+P_mP_C(1-\beta)+(1-\beta)P_mM_0\sin\psi+(1-\beta)^2M_0\sin\psi$$

$$\chi_b(\beta)=\beta+P_CP_m\beta+2\beta(1-\beta)M_0\sin\psi+\beta P_m\sin\psi,\ \chi_c(\beta)=\beta^2M_0\sin\psi$$

$$\chi_d(\beta)=P_m(1-\beta)+(1-\beta)^2,\ \chi_e(\beta)=\gamma(1-\beta)+\beta P_m+\beta(1-\beta)$$

The following simplified transformed system results from applying the finite Hankel transform to Eqs. (49) and (51) including boundary conditions (50) yield to

$$\begin{aligned}\left(\bar{f}_{CF}\right)_H(r_n,q)=&\left(\frac{\phi_2}{q}+\frac{\phi_2 y_{n11}q^{-1}}{q+y_{n10}}+\frac{\phi_2 y_{n11}q^{-1}}{q+y_{n9}}\right)\frac{J_n(r_n)}{r_n}\\&+\left(\frac{\phi_1 q}{q^2+\omega^2}\right)\left(1+\frac{y_{n11}}{q+y_{n10}}+\frac{y_{n11}}{q+y_{n9}}\right)\frac{J_n(r_n)}{r_n}\end{aligned},\tag{52}$$

and

$$\left(\bar{g}_{CF}\right)_H(r_n,q)=\left\{\frac{Y_{n13}q}{q+Y_{n14}}+\frac{Y_{n14}}{q+Y_{n14}}\right\}\left(\bar{f}_{CF}\right)_H(r_n,q),\tag{53}$$

where

$$Y_{n14}=\frac{\beta}{P_m+(1-\beta)},\ Y_{n13}=\frac{1-\beta}{P_m+(1-\beta)}\ \ Y_{n12}=\frac{Y_{n7}y_{n8}-Y_{n7}Y_{n9}-Y_{n8}Y_{n9}+Y_{n9}^2}{Y_{n10}-Y_{n9}},$$

$$Y_{n11}=\frac{Y_{n10}Y_{n7}+Y_{n10}Y_{n8}-Y_{n10}-Y_{n7}Y_{n8}}{Y_{n10}-Y_{n9}},\ Y_{n10}=\frac{Y_{n1}}{2}-\frac{Y_{n6}}{2},\ Y_{n9}=\frac{Y_{n1}}{2}+\frac{Y_{n6}}{2},\ Y_{n8}=\frac{Y_{n3}}{2}-\frac{Y_{n5}}{2},$$

$$Y_{n7}=\frac{Y_{n3}}{2}+\frac{Y_{n5}}{2},\ Y_{n6}=\sqrt{Y_{n1}^2-4Y_{n2}},\ Y_{n5}=\sqrt{Y_{n3}^2-4Y_{n4}},\ Y_{n4}=\frac{\beta^2}{\chi_d(\beta)},\ y_{n3}=\frac{\chi_e(\beta)}{\chi_d(\beta)},$$

$$Y_{n2}=\frac{-r_n^2\beta}{\chi_a(\beta)-r_n^2\chi_d(\beta)},\ Y_{n1}=\frac{\chi_b(\beta)-r_n^2\chi_e(\beta)}{\chi_a(\beta)-r_n^2\chi_d(\beta)}.$$

The application of the inverse Laplace transform to Eqs. (52) and (53) produce the time-domain solutions for the CF fractional model as:

$$\left(f_{CF}\right)_H\left(r_n,t\right)=\left(\phi_2+\phi_2 y_{n11}R_{1,1}(-y_{n10},t)+\phi_2 y_{n11}R_{1,1}(-y_{n9},t)\right)\frac{J_n\left(r_n\right)}{r_n}$$
$$+\phi_1\cos(\omega t)*\left\{\delta\left(t\right)+y_{n11}F_1(-y_{n10},t)+y_{n11}F\left(-y_{n9},t\right)\right\}\frac{J_n\left(r_n\right)}{r_n} \tag{54}$$

$$\left(g_{CF}\right)_H\left(r_n,t\right)=\left\{Y_{n13}R_{1,-1}\left(-Y_{n14},t\right)+Y_{n14}F\left(-Y_{n14},t\right)\right\}*\left(f_{CF}\right)_H\left(r_n,t\right) \tag{55}$$

This inversion approach specifically utilizes the exponential kernel characteristics of the CF derivative. Next, the application of Hankel inverse transforms to Eqs. (54) and (55) yield to:

$$f_{CF}\left(r,t\right)=2\sum_{n=1}^{\infty}\frac{J_0\left(r_1r_{1n}\right)}{r_{1n}J_1\left(r_{1n}\right)}\left[\begin{matrix}\left(\phi_2+\phi_2 y_{n11}R_{1,1}(-y_{n10},t)+\phi_2 y_{n11}R_{1,1}(-y_{n9},t)\right)\\+\phi_1\cos(\omega t)*\left\{\delta\left(t\right)+y_{n11}F_1(-y_{n10},t)+y_{n11}F_1\left(-y_{n9},t\right)\right\}\end{matrix}\right] \tag{56}$$

$$g_{CF}\left(r,t\right)=\left\{Y_{n13}R_{1,-1}\left(-Y_{n14},t\right)+Y_{n14}F_1\left(-Y_{n14},t\right)\right\}*f_{CF}\left(r,t\right) \tag{57}$$

This inversion technique reconstructs the spatial solution from its Hankel-transformed components, reinstating the radial dependence of velocity and particle distribution profiles while preserving all physical parameters and boundary effects.

4.3 Solution in terms of AB fractional operator

Equations (29) and (30) are developed using the AB fractional operator, subject to initial and boundary conditions (31) and (32), respectively. Applying the Laplace transform yields:

$$\frac{q^\gamma}{\left(1-\gamma\right)q^\gamma+\gamma}\overline{f}_{AB}\left(r,q\right)=\frac{\phi_2}{q}+\frac{\phi_1 q}{q^2+\omega^2}+\frac{d^2\overline{f}_{AB}\left(r,q\right)}{\partial r^2}+\frac{1}{r}\frac{\partial\overline{f}_{AB}\left(r,q\right)}{\partial r}$$
$$+P_C\left\{\overline{g}_{AB}\left(r,q\right)-\overline{f}_{AB}\left(r,q\right)\right\}-M_0\sin\psi\,\overline{f}_{AB}\left(r,q\right) \tag{58}$$

$$\overline{g}_{AB}\left(r,q\right)=\left\{\frac{(1-\gamma)q^\gamma+\gamma}{P_m q^\gamma+\left(1-\gamma\right)q^\gamma+\gamma}\right\}\overline{f}_{AB}\left(r,q\right) \tag{59}$$

and

$$\overline{f}_{AB}\left(1,q\right)=0,\ \overline{g}_{AB}\left(1,q\right)=0,\frac{\partial\overline{f}_{AB}\left(r,q\right)}{\partial r}\bigg|_{r=0}=0\Bigg\}. \tag{60}$$

Utilizing Eq. (59) into Eq. (58) and simplifying yields:

$$\left\{\frac{\Upsilon_a(\gamma)q^{2\gamma}+\Upsilon_b(\gamma)q^{\gamma}+\Upsilon_c(\gamma)}{\Upsilon_d(\gamma)q^{2\gamma}+\Upsilon_e(\gamma)q^{\gamma}+\gamma^2}\right\}\bar{f}_{AB}(r,q)=\frac{\phi_2}{q}+\frac{\phi_1 q}{q^2+\omega^2}+\frac{d^2\bar{f}_{AB}(r,q)}{\partial r^2}+\frac{1}{r}\frac{\partial\bar{f}_{AB}(r,q)}{\partial r}, \quad (61)$$

where

$$\Upsilon_a(\gamma)=P_m+(1-\gamma)+P_mP_C(1-\gamma)+(1-\gamma)P_mM_0\sin\psi+(1-\gamma)^2M_0\sin\psi$$

$$\Upsilon_b(\gamma)=\gamma+P_CP_m\gamma+2\gamma(1-\gamma)M_0\sin\psi+\gamma P_m\sin\psi,\ \Upsilon_c(\gamma)=\gamma^2M_0\sin\psi$$

$$\Upsilon_d(\gamma)=P_m(1-\gamma)+(1-\gamma)^2,\ \Upsilon_e(\gamma)=\gamma(1-\gamma)+\gamma P_m+\gamma(1-\gamma)$$

The finite Hankel transform applied to Eqs. (59) and (61) with boundary conditions (60) yields the following simplified form:

$$\left(\bar{g}_{AB}\right)_H(r_n,q)=\left\{\frac{Z_{n13}q^{\gamma}}{q^{\gamma}+Z_{n14}}+\frac{Z_{n14}}{q^{\gamma}+Z_{n14}}\right\}\left(\bar{f}_{AB}\right)_H(r_n,q), \quad (62)$$

and

$$\begin{aligned}\left(\bar{f}_{AB}\right)_H(r_n,q)=&\left(\frac{\phi_2}{q}+\frac{\phi_2Z_{n11}q^{-1}}{q^{\gamma}+Z_{n10}}+\frac{\phi_2Z_{n11}q^{-1}}{q^{\gamma}+Z_{n9}}\right)\frac{J_n(r_n)}{r_n}\\&+\left(\frac{\phi_1 q}{q^2+\omega^2}\right)\left(1+\frac{Z_{n11}}{q^{\gamma}+Z_{n10}}+\frac{Z_{n11}}{q^{\gamma}+Z_{n9}}\right)\frac{J_n(r_n)}{r_n}\end{aligned}, \quad (63)$$

where

$$Z_{n14}=\frac{\gamma}{\Phi_m+(1-\gamma)},\qquad Z_{n13}=\frac{1-\gamma}{\Phi_m+(1-\gamma)},\qquad Z_{n12}=\frac{Z_{n7}Z_{n8}-Z_{n7}Z_{n9}-Z_{n8}Z_{n9}+Z_{n9}^2}{Z_{n10}-Z_{n9}},$$

$$Z_{n11}=\frac{Z_{n10}Z_{n7}+Z_{n10}Z_{n8}-Z_{n10}-Z_{n7}Z_{n8}}{Z_{n10}-Z_{n9}},\quad Z_{n10}=\frac{Z_{n1}}{2}-\frac{Z_{n6}}{2},\quad Z_{n9}=\frac{Z_{n1}}{2}+\frac{Z_{n6}}{2},\ Z_{n8}=\frac{Z_{n3}}{2}-\frac{Z_{n5}}{2},$$

$$Z_{n7}=\frac{Z_{n3}}{2}+\frac{Z_{n5}}{2},\ Z_{n6}=\sqrt{Z_{n1}^2-4Z_{n2}},\quad Z_{n5}=\sqrt{Z_{n3}^2-4Z_{n4}},\quad Z_{n4}=\frac{\gamma^2}{\Upsilon_d(\gamma)},\quad Z_{n3}=\frac{\Upsilon_e(\gamma)}{\Upsilon_d(\gamma)},$$

$$Z_{n2}=\frac{-r_n^2\gamma}{\Upsilon_a(\gamma)-r_n^2\Upsilon_d(\gamma)},\ Z_{n1}=\frac{\Upsilon_b(\gamma)-r_n^2\Upsilon_e(\gamma)}{\Upsilon_a(\gamma)-r_n^2\Upsilon_d(\gamma)}.$$

The use of the inverse Laplace transform on Eqs. (62) and (63) yields the following time-domain solutions:

$$\left(g_{AB}\right)_H\left(r_n,t\right)=\left\{Z_{n13}R_{\gamma,-\gamma}\left(-Z_{n14},t\right)+Z_{n14}F_{\gamma}\left(-Z_{n14},t\right)\right\}*\left(f_{AB}\right)_H\left(r_n,t\right), \tag{64}$$

$$\begin{aligned}\left(f_{AB}\right)_H\left(r_n,t\right)=&\left(\phi_2+\phi_2 Z_{n11}R_{\gamma,1}\left(Z_{n10},t\right)+\phi_2 Z_{n11}R_{\gamma,1}\left(Z_{n9},t\right)\right)\frac{J_n\left(r_n\right)}{r_n}\\&+\phi_1\cos(\omega t)*\left\{\delta\left(t\right)+Z_{n11}F_{\gamma}\left(Z_{n10},t\right)+Z_{n11}F_{\gamma}\left(-Z_{n9},t\right)\right\}\frac{J_n\left(r_n\right)}{r_n}\end{aligned}. \tag{65}$$

This inversion method notably employs the properties of the Mittag-Leffler kernel with the AB derivative. Meanwhile, the application of Hankel inverse transformations to Eqs. (64) and (65) results in:

$$g_{AB}\left(r,t\right)=\left\{Z_{n13}R_{\gamma,-\gamma}\left(-Z_{n14},t\right)+Z_{n14}F_{\gamma}\left(-Z_{n14},t\right)\right\}*f_{AB}\left(r,t\right), \tag{66}$$

$$f_{AB}\left(r,t\right)=2\sum_{n=1}^{\infty}\frac{J_0\left(r_1r_{1n}\right)}{r_{1n}J_1\left(r_{1n}\right)}\left[\begin{aligned}&\phi_2+\phi_2 Z_{n11}R_{\gamma,1}\left(Z_{n10},t\right)+\phi_2 Z_{n11}R_{\gamma,1}\left(Z_{n9},t\right)\\&+\phi_1\cos(\omega t)*\left\{\delta\left(t\right)+Z_{n11}F_{\gamma}\left(Z_{n10},t\right)+Z_{n11}F_{\gamma}\left(-Z_{n9},t\right)\right\}\end{aligned}\right]. \tag{67}$$

5. Limiting cases

This section presents the reduction of the solutions resulting from Eqs. (44) and (45) to classical form and validate them against previously published research.

5.1. Case I: For Classical Magnetic Blood Flow Utilizing Brinkman Type Fluid Model when $\alpha\to 1$

By establishing $\alpha\to 1$, the functions of Lorenzo and Hartleys, as well as Robotnov and Hartleys, are respectively simplified to the following forms [31].

$$R_{1,-1}\left(-\xi,t\right)=\sum_{k=0}^{\infty}\frac{\left(-\xi\right)^k t^{k+1}}{k!}=L^{-1}\left\{\frac{q^{-1}}{q+\xi}\right\}=\frac{1-e^{\eta t}}{\xi}, \tag{68}$$

$$F_1\left(-\xi,t\right)=\sum_{k=0}^{\infty}\frac{\left(-\xi\right)^k t^{k}}{k!}=L^{-1}\left\{\frac{1}{q+\xi}\right\}=e^{-\eta t}, \tag{69}$$

that lead $X\left(\tau\right)$ and $Y\left(\tau\right)$ as provided in Eq. (41) to $X_1\left(\tau\right)$ and $Y_1\left(\tau\right)$ as follow:

$$X_1(\tau)\big|_{\alpha=1} = \frac{\phi_2}{d_{2n}}\left\{\frac{d_{2n}}{r_n{}^2 - M_0} - \frac{1-P_m}{d_{4n}}e^{-d_{4n}\tau} + \frac{1-P_m}{d_{3n}}e^{-d_{3n}\tau}\right\}, \tag{70}$$

$$Y_1(\tau)\big|_{\alpha=1} = \frac{\phi_1}{d_{2n}}\left\{\begin{array}{l}\frac{1-P_m d_{n4}}{d_{n4}{}^2 - \omega_1^2}\left(d_{n4}\cos\omega_1\tau + \omega_1\sin\omega_1\tau - d_{n4}e^{-d_{n4}\tau}\right) \\ -\frac{1-P_m d_{n3}}{d_{n3}{}^2 - \omega_1^2}\left(d_{n3}\cos\omega_1\tau + \omega_1\sin\omega_1\tau - d_{d_{n3}}e^{-d_{n3}t}\right)\end{array}\right\}. \tag{71}$$

Eventually, Eqs. (46) and (47) have been simplified to the subsequent classical solutions:

$$f(r,\tau) = 2\sum_{n=1}^{\infty}\frac{J_0(rr_n)}{r_n J_1(r_n)}\left\{X_1(\tau)\big|_{\alpha=1} + Y_1(\tau)\big|_{\alpha=1}\right\}, \tag{72}$$

and

$$g(r,\tau) = \frac{1}{p_m}\int_0^{\tau} e^{-p_m s} f(r,\tau-s)\,ds\,. \tag{73}$$

5.2. Case II: For Classical Magnetic Blood Flow Model when $\beta_1 \to 0$

By setting $\beta_1 \to 0$, the solutions derived from Eq. (72) and (73) are simplified to the following Classical form.

$$f_1(r,\tau) = 2\sum_{n=1}^{\infty}\frac{J_0(rr_n)}{r_n J_1(r_n)}\left\{X_2(\tau) + Y_2(\tau)\right\}, \tag{74}$$

$$g_1(r_1,\tau) = \frac{1}{p_m}\int_0^{\tau} e^{-p_m s} f(r,\tau-s)\,ds\,, \tag{75}$$

where

$$X_2(\tau) = \frac{\phi_2}{d_{2n}}\left\{\frac{c_{2n}}{r_n{}^2 - M_0} - \frac{1-P_m}{c_{4n}}e^{-d_{4n}\tau} + \frac{1-P_m}{c_{3n}}e^{-d_{3n}\tau}\right\}, \tag{76}$$

$$Y_2(\tau) = \frac{\phi_1}{c_{2n}}\left\{\begin{array}{l}\frac{1-P_m c_{n4}}{d_{n4}{}^2 - \omega_1^2}\left(c_{n4}\cos\omega_1\tau + \omega_1\sin\omega_1\tau - c_{n4}e^{-d_{n4}\tau}\right) \\ -\frac{1-P_m c_{n3}}{c_{n3}{}^2 - \omega_1^2}\left(c_{n3}\cos\omega_1\tau + \omega_1\sin\omega_1\tau - c_{d_{n3}}e^{-d_{n3}t}\right)\end{array}\right\}. \tag{77}$$

$$c_{n1}=\left\{1+P_m\left(P_C+M\right)+r_{1n}{}^2P_m\right\},\ c_{n2}=\sqrt{\left(c_{1n}\right)^2-4P_m\left(r_{1n}{}^2+M\right)},\ c_{n3}=\frac{c_{n1}+c_{n2}}{2P_m},c_{n4}=\frac{c_{n1}-c_{n2}}{2P_m}$$

The solutions derived in Eqs. (74) and(75) of this study are graphically compared with the previously published findings of Zafar *et al.* [43] [Eqs. (23)-(26)] in Figure 2(a,b). The entire overlap of both solution curves reveals exact agreement between present solutions and established results, confirming the mathematical validity of our results.

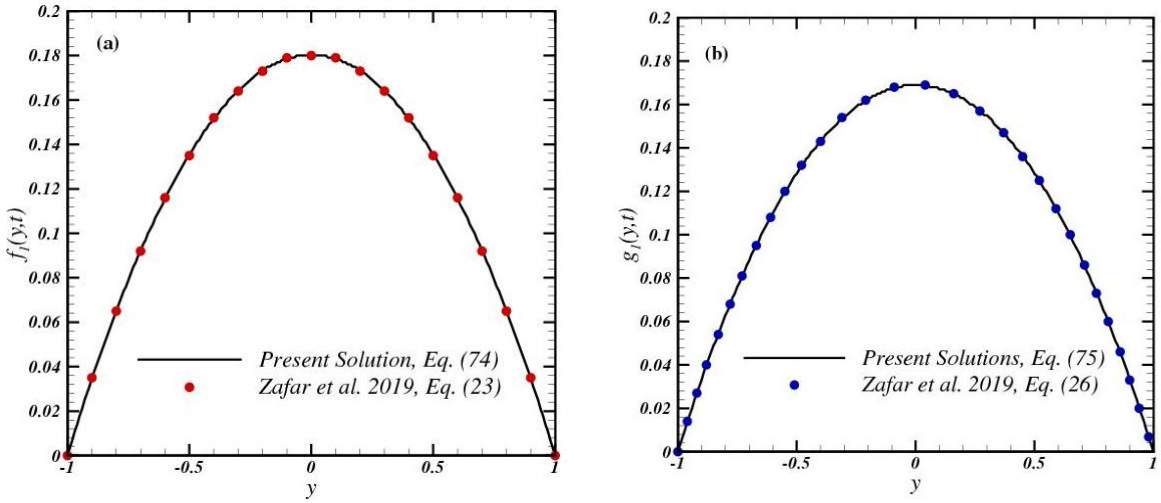


Figure 2: The current solutions outlined in Eqs. (74) and (75) are compared with those derived by *Zafar et al.* 2019, specifically Eqs. (23) and (26).

6. Results and Discussion

The research examines the two-phase flow of blood containing magnetic particles in a slender cylindrical tube. Due to the highly porous characteristics of capillary walls, the Brinkman-type fluid model is utilized to accurately represent the flow behavior, as it incorporates both viscous and porous medium aspects. To enhance the model's physical realism and account for memory effects, the classical blood flow equations are generalized using three distinct fractional derivative operators: the Caputo, CF, and AB versions. Each of these fractional operators introduces unique memory kernels, power-law, exponential, and Mittag-Leffler, facilitating a more comprehensive investigation of flow dynamics in contrast to standard integer-order models. Exact analytical results for both blood and magnetic particle velocities are obtained through an advanced mathematical method that integrates Laplace and finite Hankel transforms, effectively addressing

fractional operators and cylindrical geometry. These general solutions are reduced to their corresponding classical counterparts when $\alpha \to 1$, providing a crucial validation of the model's consistency. The study conducts comprehensive analyses to systematically investigate the impact of various physical parameters on flow characteristics, including the α, β, γ , t β_1, M , P_C , and P_m . The physical influence of each parameter is analyzed to clarify their individual and combined effects on the velocity profiles of blood and magnetic particles.

6.1. Blood and magnetic particle velocities as affected by α, β , and γ

Figure 3 [I(a, b), II(a, b), and III(a, b)] illustrates the impact of the fractional parameters α, β , and γ on the velocities of blood and magnetic particles over a longer period ($t = 1.5$), comparing the Caputo, Caputo-Fabrizio, and Atangana-Baleanu fractional operators. Blood and particle velocities increase with rising values of α, β , and γ , reaching their maximum when these parameters equal 1. This occurs as elevated fractional orders enhance momentum diffusion, resulting in a thicker boundary layer that facilitates more rapid fluid movement. At the maximum fractional order ($\alpha, \beta, \gamma = 1$), the flow resembles the standard blood flow model, characterized by maximum momentum transfer efficiency. The dispersed magnetite particles exhibit this pattern due to their mobility being intimately linked to the blood flow. This behavior corresponds with prior research, including Azhar *et al.* [44], which demonstrated that fractional derivatives can influence flow dynamics by modifying diffusion rates.

Nonetheless, at short durations (*t = 0.2*), as illustrated in Figure 4 [I(a, b), II(a, b), and III(a, b)], the behavior inverts velocities diminish with rising α, β, and γ. This occurs because, in the initial phases, fractional derivatives induce memory effects that impede rapid acceleration. Increased fractional orders exert more pronounced non-local dependencies, indicating that the fluid remembers its previous condition more acutely, hence decelerating the initial flow development. This dual behavior, in which fractional parameters initially suppress and subsequently augment velocities, has been confirmed by Shah *et al.* [45] and Ali *et al.* [25], demonstrating that fractional models more precisely describe time-dependent flow transitions compared with standard approaches.

To further examine this phenomenon, Figure 5 I(a, b), II(a, b), and III(a, b)] plot velocities against time, highlighting a pivotal transition point (about $t = 0.3$) where the fractional effects

move from deceleration to acceleration of the flow. Each fractional operator, Caputo, CF, and AB, demonstrates subtle distinctions in this transition owing to their varied memory kernels. The power-law kernel used by Caputo may result in singularities, whereas the exponential kernel used by CF avoids this problem and produces more consistent short-term behavior. An enhanced representation that accurately reflects short- and long-term memory effects is provided by the AB Mittag-Leffler kernel.

In summary, the parameters α, β, and γ employ a extensive effect on the velocity fields of both blood and MNPs, however their influences are time-dependent. Higher values of α, β, and γ mostly improve flow by promoting momentum diffusion over extended timescales. On the other hand, flow is delayed by memory-induced resistive impact leading at shorter intervals. With a more realistic results framework than traditional integer-order models, this dual performance highlights the critical role fractional calculus plays in capturing intricate bio-magnetic interactions. Additionally, comparing several fractional operators highlights how crucial it is to choose a model that is appropriate for a given flow regime and set of application needs

6.2. Blood and magnetic particle velocities as affected by β_1

Figure 6 [I(a, b), II(a, b), III(a, b)] illustrates how the β_1 affects the velocities of blood and magnetic particles. In each case, time is fixed at *t=0.5*, and the α, β, and γ are held constant. It is clear from the results that a significant drop in the velocities of magnetic and blood particles occurs in tandem with an increase in the β_1. More resistance to flow within the porous structure of blood arteries is indicated by higher values of the β_1, which is the ratio of viscous forces to permeability effects in porous media. As a result of this greater resistance, the blood and suspended particles experience higher drag forces, which slows their flow.

The relationship between the β_1 and flow velocity can be elucidated using the governing equations (Eq. 12), wherein the β_1 manifests as an extra resistance component proportionate to the velocity. As β_1 increases, drag forces become more pronounced, resulting in enhanced energy dissipation and subsequently diminished velocities. This behavior is uniform among the three fractional models (Caputo, CF, AB), although minor discrepancies may occur due to the distinct approaches each fractional operator employs in addressing memory effects. The Caputo model's

power-law memory kernel demonstrates a more progressive decrease in velocities than the exponential kernel of CF or the Mittag-Leffler kernel of AB, however, the overarching tendency persists. The observed retardation effect corresponds with earlier studies by Jan *et al.* [46], who documented analogous velocity suppression in Brinkman-type flow utilizing the Caputo Fractional operator.

6.3. Blood and magnetic particle velocities as affected by M

Figure 6 [I(a, b), II(a, b), and III(a, b)] provide a comprehensive analysis of the impact of the M on the velocities of blood and magnetic particles. The findings indicate a steady reduction in both blood and magnetic particle velocities with an increase in the M . This phenomenon arises as the applied magnetic field generates Lorentz forces that counteract the flow direction, resulting in a resistive effect akin to increased drag. When blood, an electrically conductive fluid containing magnetic particles, flows within a magnetic field, the interaction between the field and the moving charges produces Lorentz forces. The magnitude of this braking effect is exactly related to the intensity of the magnetic field, formally denoted by M (magnetic parameter). As M increases, the Lorentz forces become more pronounced, resulting in heightened resistance to the flow and subsequently diminishing velocities. This behavior is consistently observed across all three fractional models (Caputo, CF and AB), but nuanced discrepancies may arise in the rate of velocity decay attributable to their unique memory kernel characteristics.

The result has significant implications for medicinal applications such as magnetic drug targeting, where meticulous control over particle motion is crucial. By modulating magnetic field intensity, doctors might theoretically control the velocity of therapeutic particles in the bloodstream, potentially enhancing localized delivery of drugs while reducing systemic dispersion.

6.4. Blood and magnetic particle velocities as affected by P_C

The effect of the P_C on the velocities of blood and magnetic particles is thoroughly examined in Figures 7 [I(a, b), II(a, b), and III(a, b)]. The results indicate a clear deceleration effect, wherein both blood and magnetic particle velocities diminish progressively with elevated particle concentration. This observed tendency confirms earlier findings by Nandkeolyar and Das [47],

affirming that elevated P_C fundamentally modify the rheological properties of the blood-particle suspension.

This pattern of behavior arises from two interconnected causes from a physical perspective. Initially, when the P_C escalates, the effective viscosity of blood markedly increases. The suspended particles provide increased internal friction inside the fluid, necessitating higher energy input to sustain the same flow velocity. Secondly, the augmented particle loading elevates the overall density of the suspension, rendering the fluid more resistant to inertial acceleration. The two processes together result in a significant reduction in velocity during both stages of the flow, with the magnetic particles undergoing marginally more deceleration due to their direct interaction with the carrier fluid.

6.5. Blood and magnetic particle velocities as affected by P_m

The impact of P_m on the velocities of blood and magnetic particles is comprehensively analyzed in Figures 8 [I(a, b), II(a, b), and III(a, b)]. The results indicate a consistent retardation effect, wherein both blood flow and magnetic particle velocities diminish progressively with increasing P_m. This observed result agrees with earlier findings by Nandkeolyar and Das [47], affirming that P_m is pivotal in influencing the dynamic behavior of the blood-particle suspension system.

This behavior can be understood through various interconnected mechanisms from a fundamental physics standpoint. Initially, when P_m increases, their inertial resistance to acceleration escalates correspondingly in accordance with Newton's second law. This necessitates a greater force to achieve comparable acceleration, leading to reduced velocities for a given driving pressure gradient. Secondly, P_m increasing generates more substantial hydrodynamic interactions with the surrounding blood plasma, hence enhancing the system's apparent viscosity through increased particle-fluid momentum transfer. Third, P_m when increases the total density of the suspension, making the fluid more resistive to its initial creation and maintenance of flow.

The framework of fractional calculus offers a deeper understanding of how various timeframes affect flow dynamics. While all three fractional operators exhibit a comparable qualitative trend in velocity reduction, they display subtle differences in the temporal evolution of

this retardation. The Caputo derivative, with a power-law memory kernel, predicts a more gradual decrease in velocity as P_m grows, signifying long-term memory effects inside the system. Conversely, the CF model, characterized by an exponential memory kernel, exhibits a more prompt reaction to mass alterations, effectively encapsulating short-term inertial effects. The AB operator, which integrates the Mittag-Leffler memory function, reconciles two extremes by concurrently addressing both short- and long-term memory effects.

7. Concluding remarks

The research examines unsteady two-phase blood flow with magnetic particles in a slant cylindrical vessel influenced by magnetic fields. The analysis utilizes the Brinkman fluid model for blood flow, Maxwell's equations for magnetic field interactions, Newton's second law for particle motion, and three fractional operators (Caputo, CF, and AB) to generalize the governing equations. Exact analytical solutions are obtained through the combination of Laplace and Hankel transforms, with classical solutions emerging as $\alpha, \beta, \gamma \to 1$. The main findings of this investigation are summarized as follows.

- Blood and magnetic particle velocities diminish with increasing M due to counteracting Lorentz forces, with CF demonstrating the promptest reaction, while AB reflects an intermediate effect.
- The rise of P_C diminishes flow velocities, as an increased particle density raises effective blood viscosity and flow resistance.
- The P_m exhibits an inverse correlation with velocities; heavier particles result in slower flows due to increased inertial resistance and augmented drag forces.
- The α, β and γ demonstrate dual time-dependent behavior: they increase velocities at extended durations ($t > 0.3$) while initially suppressing them, with transition dynamics differing by operator type.
- Increases in β_1 lead to reductions in velocity by enhancing the resistance of the porous medium, particularly evident in the results of the Caputo model.
- The AB solutions optimally align with anticipated physiological responses by concurrently incorporating short-term inertial effects and long-term memory attributes.

- Classical integer-order models ($\alpha, \beta, \gamma \to 1$) consistently overestimate velocities in comparison to fractional solutions, underscoring the significance of fractional calculus.
- Magnetic particles exhibit a more significant reduction in velocity compared to blood plasma under equivalent conditions, attributable to direct interactions with the Lorentz force.
- The research delineates criteria for selecting fractional operators: Caputo for long-term forecasts, CF for immediate effects, and AB for comprehensive analysis

Competing Interests

The authors declare no competing interest regarding this publication.

Data Availability Statement

The data that support the findings of this study are available from the corresponding author upon reasonable request.

Ethics approval

The entire work is the original work of the authors.

Consent for publication

All the authors have given their consent to publish the paper. Authors Contributions.

Funding declaration: This work received no external funding.

Author Contributions

M.S: Conceptualization, Methodology, Validation, Writing - Original Draft, Supervision. **M.J and Z.K**: Formal analysis, Investigation, Data Curation, Writing - Original Draft, Visualization. **M.B** and **M.S**: Investigation, Resources, Writing - Review & Editing. **M.J, M.B and ZK**: Methodology, Software, Validation, Writing - Review & Editing.

Acknowledgement

The authors extend their appreciation to the Deanship of Scientific Research at Northern Border University, Arar, KSA for funding this research work through the project number "NBU-FFR-2025-2942-XX"

.

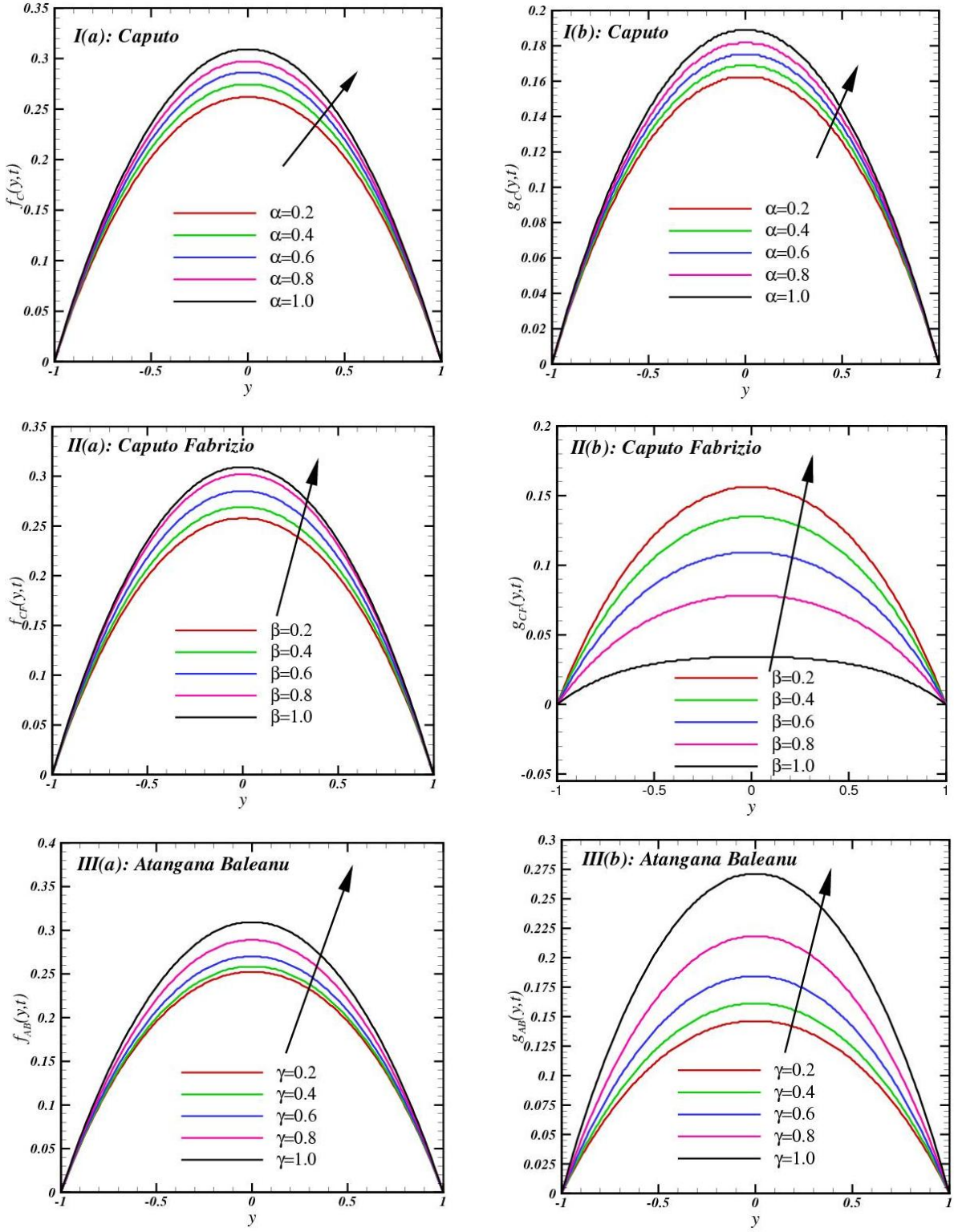


Figure 3: Velocities dependence on α, β and γ for $t = 1.5$

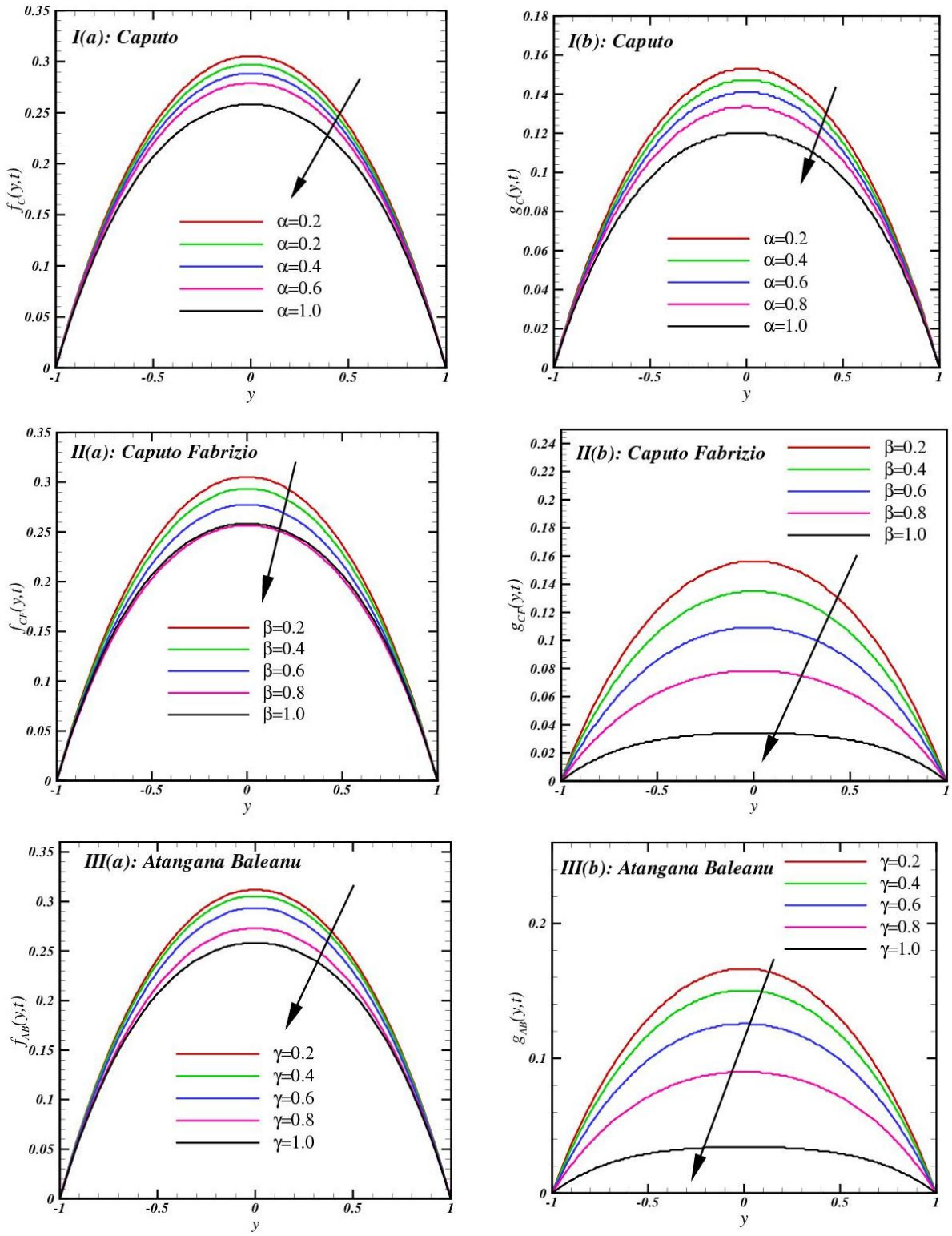


Figure 4: Velocities dependence on α, β and γ for $t = 0.2$

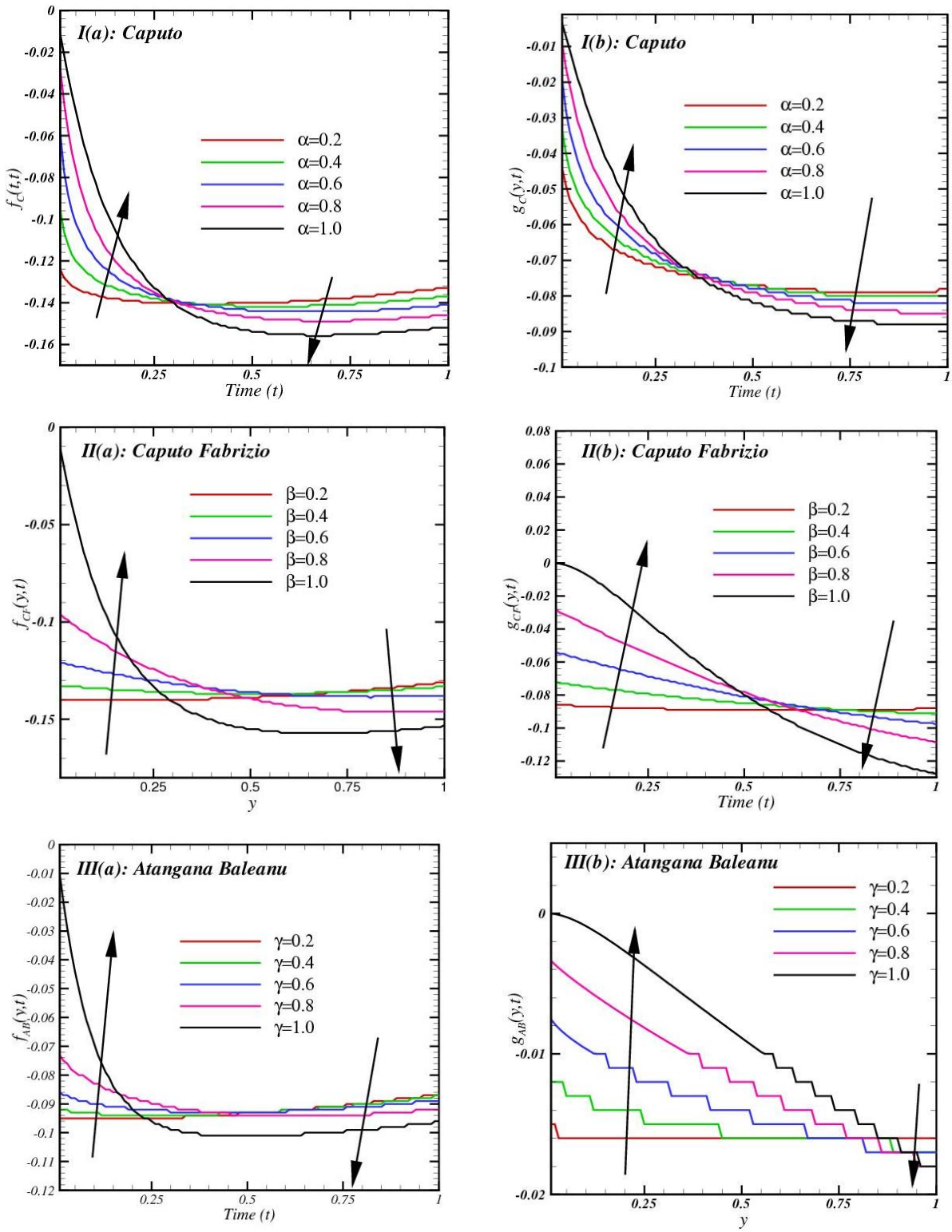


Figure 5: Velocities dependence on α, β and γ against t

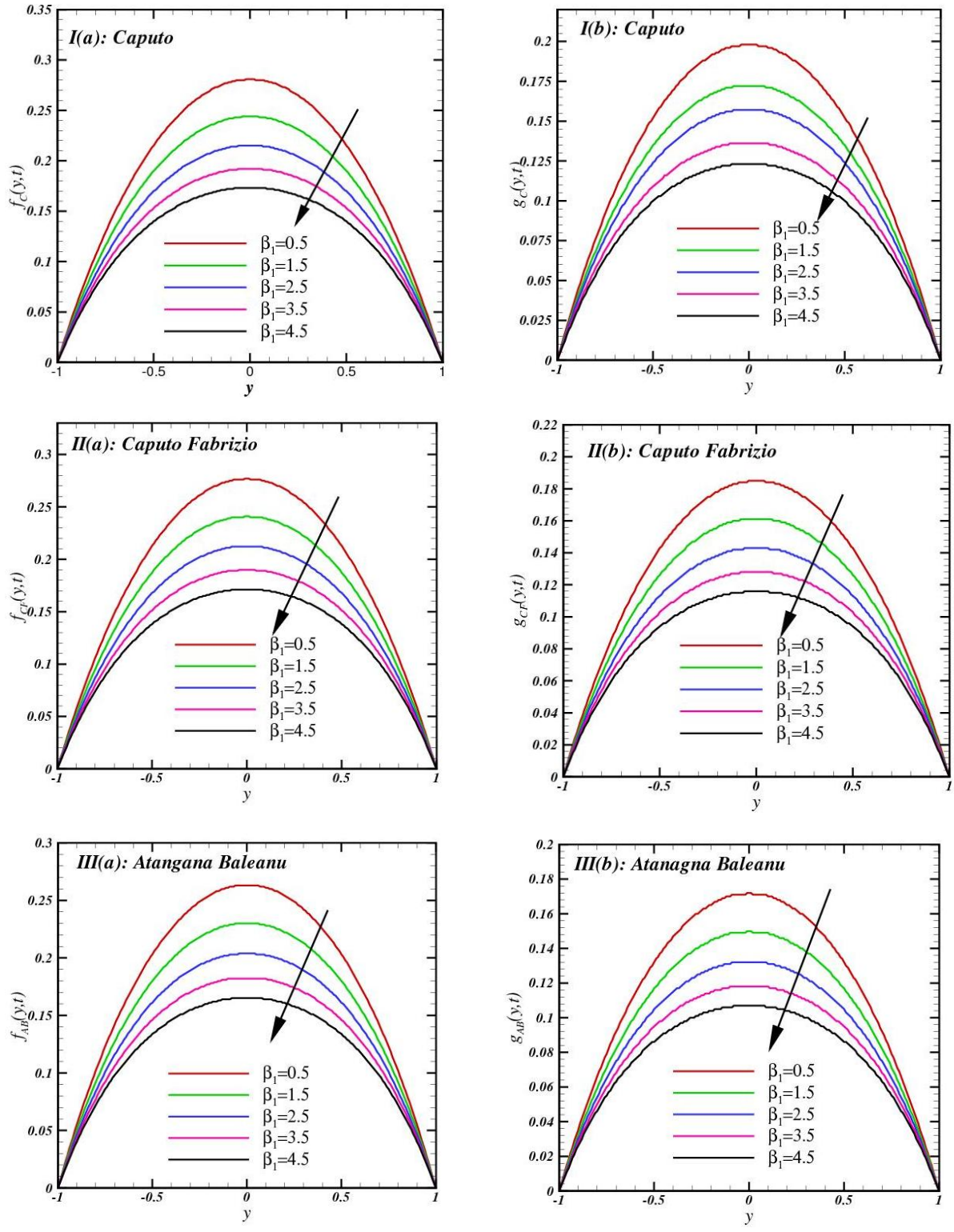


Figure 6: Velocities dependence on β_1

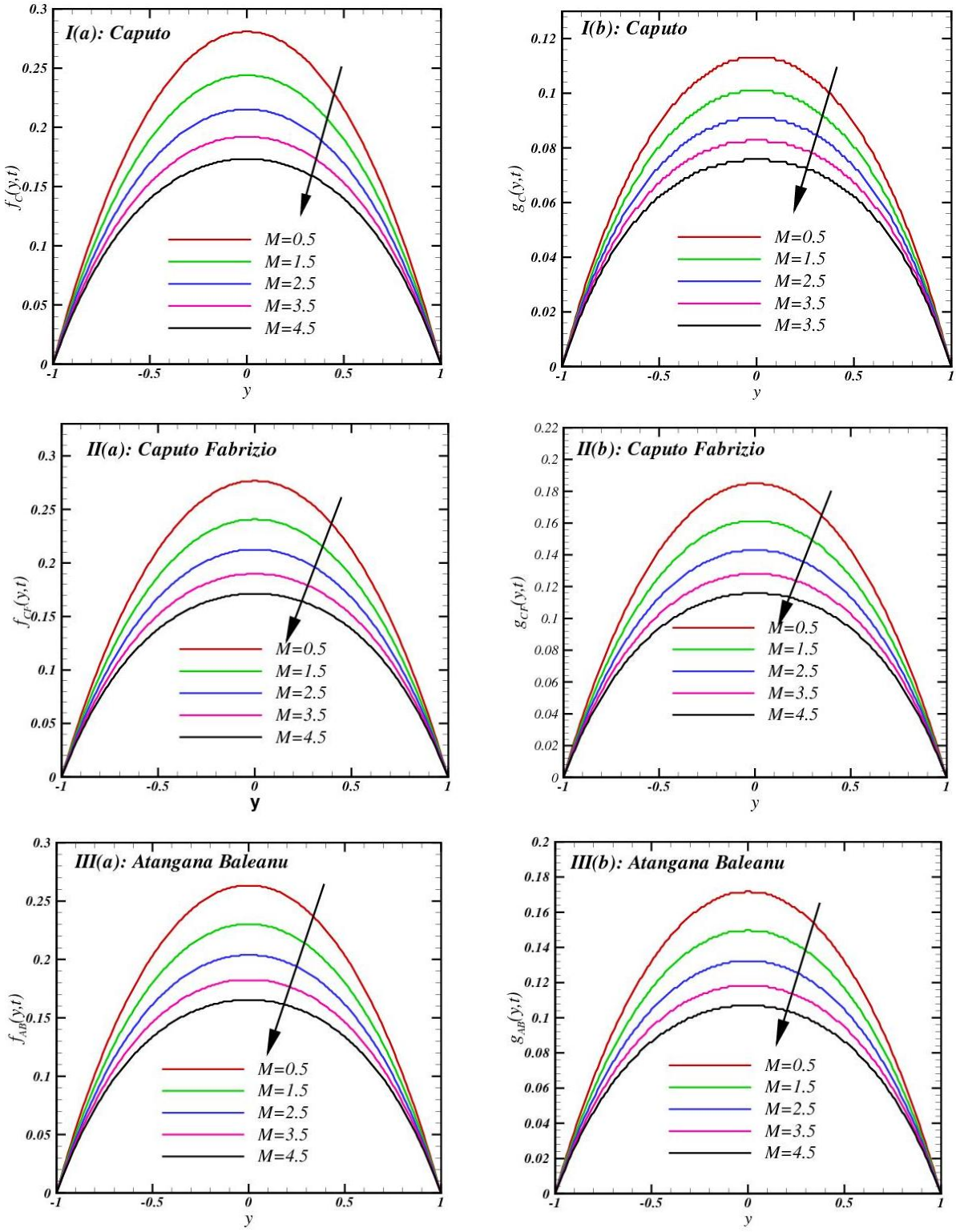


Figure 7: Velocities dependence on M

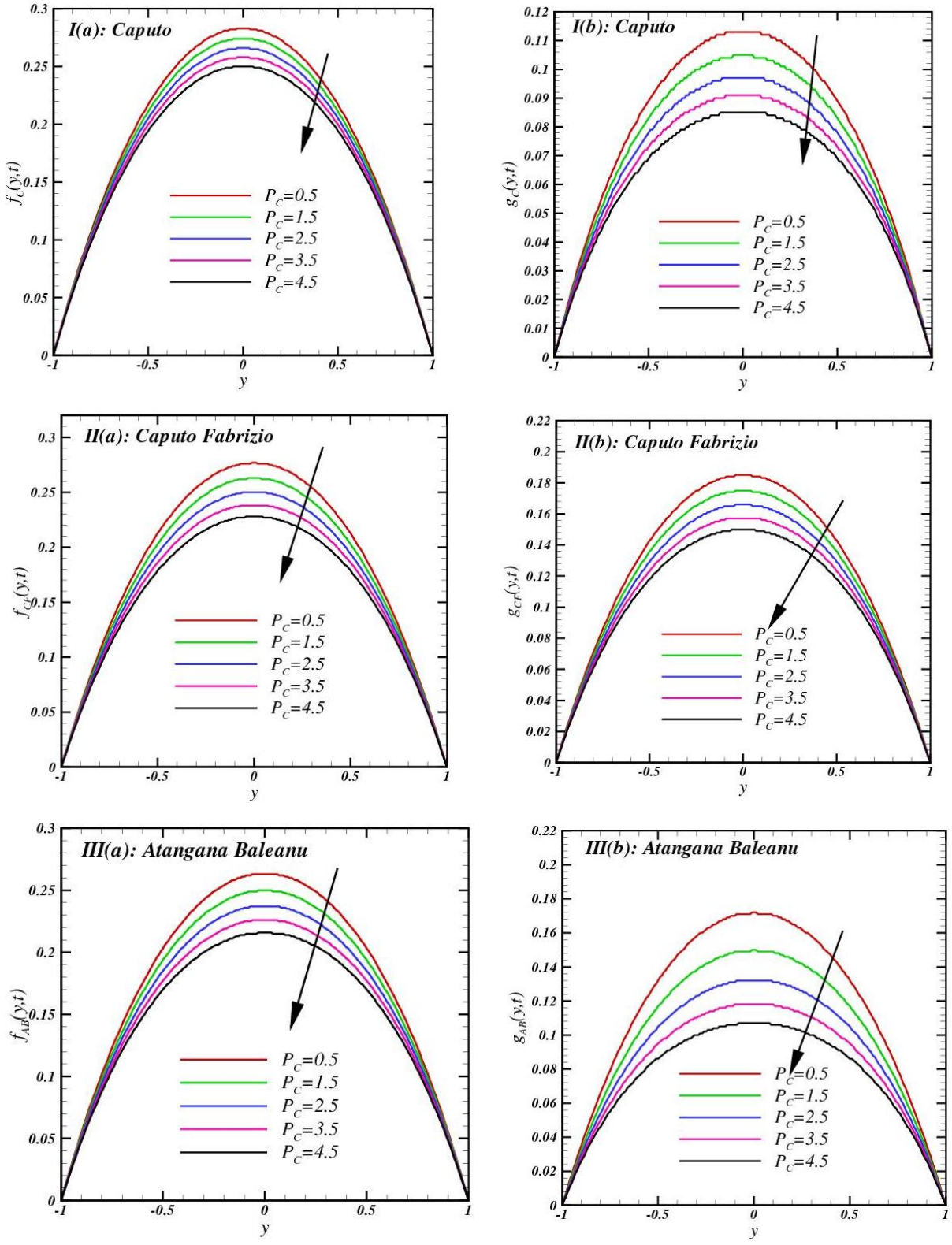


Figure 8: Velocities dependence on P_C

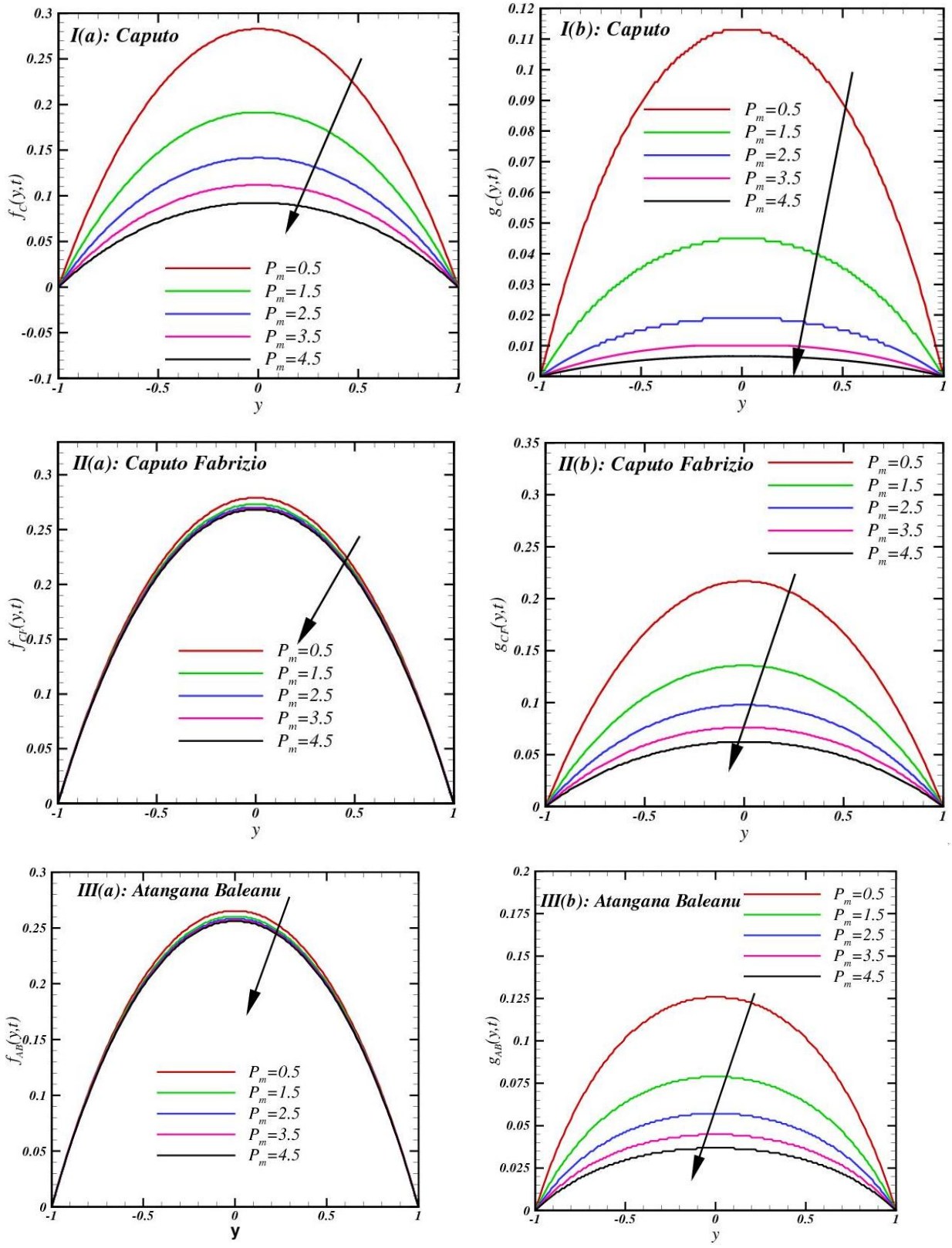


Figure 9: Velocities dependence on P_m

References

1. Haik, Y., V. Pai, and C.-J. Chen, *Development of magnetic device for cell separation.* Journal of Magnetism and Magnetic Materials, 1999. **194**(1-3): p. 254-261.
2. Tzirtzilakis, E.E., *A mathematical model for blood flow in magnetic field.* Physics of fluids, 2005. **17**(7).
3. Murtaza, M.G., E.E. Tzirtzilakis, and M. Ferdows, *Effect of electrical conductivity and magnetization on the biomagnetic fluid flow over a stretching sheet.* Zeitschrift für angewandte Mathematik und Physik, 2017. **68**: p. 1-15.
4. Javeed, S. and I.H. Jung, *Numerical analysis of the behavior of two-phase blood flow in locally magnetized vessel.* Chinese Journal of Physics, 2023. **86**: p. 497-507.
5. Chrimatopoulos, G., E.E. Tzirtzilakis, and M.A. Xenos, *Magnetohydrodynamic and Ferrohydrodynamic Fluid Flow Using the Finite Volume Method.* Fluids, 2023. **9**(1): p. 5.
6. Könözsy, L., P. Scienza, and D. Drikakis, *Validation of a magneto-and ferro-hydrodynamic model for non-isothermal flows in conjunction with Newtonian and non-Newtonian fluids.* 2016.
7. Kasiman, E.H., et al., *Mixed finite element formulation for Navier–Stokes equations for magnetic effects on biomagnetic fluid in a rectangular channel.* Materials, 2022. **15**(8): p. 2865.
8. Rajashekhar, C., G. Manjunatha, and K.S. Basavarajappa, *Analytical solution of FHD flow of blood through two layered model in the presence of magnetic field.* Journal of Mechanical Engineering Research and Developments, 2017. **40**(2): p. 365-370.
9. Fenech, M. and L. Haya, *Blood flow mechanics.* Cardiovascular Mechanics, 2018: p. 63-89.
10. Gregory, T.S., et al., *The magnetohydrodynamic effect and its associated material designs for biomedical applications: a state-of-the-art review.* Advanced Functional Materials, 2016. **26**(22): p. 3942-3952.
11. Drochon, A., M. Beuque, and D.D.R.A.-A. Rodriguez, *A review of some reference analytic solutions for the magnetohydrodynamic flow of blood.* Applied Mathematics, 2018. **9**(10): p. 1179-1192.
12. Nisar, K.S., et al., *A review of fractional order epidemic models for life sciences problems: Past, present and future.* Alexandria Engineering Journal, 2024. **95**: p. 283-305.

13. Magin, R., *Fractional calculus in bioengineering, part 1.* Critical Reviews™ in Biomedical Engineering, 2004. **32**(1).
14. Failla, G. and M. Zingales, *Advanced materials modelling via fractional calculus: challenges and perspectives.* Philosophical Transactions of the Royal Society A, 2020. **378**(2172): p. 20200050.
15. Podlubny, I., *Fractional differential equations: an introduction to fractional derivatives, fractional differential equations, to methods of their solution and some of their applications*. Vol. 198. 1998: elsevier.
16. Caputo, M. and M. Fabrizio, *A new definition of fractional derivative without singular kernel.* Progress in Fractional Differentiation & Applications, 2015. **1**(2): p. 73-85.
17. Atangana, A. and D. Baleanu, *New fractional derivatives with nonlocal and non-singular kernel: theory and application to heat transfer model.* arXiv preprint arXiv:1602.03408, 2016.
18. Soong, D.S., *Time Dependent Nonlinear Viscoelastic Behavior of Polymer Fluids—A Review of Current Understanding.* Rubber Chemistry and Technology, 1981. **54**(3): p. 641-661.
19. Magin, R.L., *Fractional calculus models of complex dynamics in biological tissues.* Computers & Mathematics with Applications, 2010. **59**(5): p. 1586-1593.
20. Dos Santos, M.A.F., *Analytic approaches of the anomalous diffusion: A review.* Chaos, Solitons & Fractals, 2019. **124**: p. 86-96.
21. Shaikh, A., et al., *Analysis of differential equations involving Caputo–Fabrizio fractional operator and its applications to reaction–diffusion equations.* Advances in Difference Equations, 2019. **2019**(1): p. 1-14.
22. Li, C., L. Zheng, and T. He, *Fractional-order rate-dependent porous-thermo-elasticity model based on new fractional derivatives with non-singular kernels and 1D transient dynamic response analysis of magnesium-based porous half-space with voids.* Archive of Applied Mechanics, 2025. **95**(1): p. 1-28.
23. Hristov, J., *Derivatives with non-singular kernels from the Caputo-Fabrizio definition and beyond: Appraising analysis with emphasis on diffusion models*, in *Frontiers in fractional calculus*. 2018, Bentham Science Publishers. p. 269-341.

24. Alkahtani, B.S.T., *Dynamical Analysis of Rubella Disease Model in the Context of Fractional Piecewise Derivative: Simulations with Real Statistical Data.* Fractal and Fractional, 2023. **7**(10): p. 746.
25. Ali, F., et al., *Magnetic field effect on blood flow of Casson fluid in axisymmetric cylindrical tube: A fractional model.* Journal of Magnetism and Magnetic Materials, 2017. **423**: p. 327-336.
26. Riaz, M.B. and A.A. Zafar, *Exact solutions for the blood flow through a circular tube under the influence of a magnetic field using fractional Caputo-Fabrizio derivatives.* Mathematical Modelling of Natural Phenomena, 2018. **13**(1): p. 8.
27. Saikia, D., U.K. Saha, and G.C. Hazarika, *Atangana-Baleanu and Caputo-Fabrizio Analysis of Fractional Derivatives on MHD Flow past a Moving Vertical Plate with Variable Viscosity and Thermal Conductivity in a Porous Medium.* International Journal of Mathematical, Engineering and Management Sciences, 2021. **6**(2): p. 493.
28. Saikia, D., U.K. Saha, and G.C. Hazarika. *A Numerical Study on Atangana–Baleanu and Caputo–Fabrizio Analysis of Fractional Derivatives for the Effects of Variable Viscosity and Thermal Conductivity on an MHD Flow Over a Vertical Hot Stretching Sheet with Radiation and Viscous Dissipation*. Springer.
29. Sheikh, N.A., et al., *A comparative study of Atangana-Baleanu and Caputo-Fabrizio fractional derivatives to the convective flow of a generalized Casson fluid.* The European Physical Journal Plus, 2017. **132**: p. 1-14.
30. Bouzenna, F.E.-G., M.T. Meftah, and M. Difallah, *Application of the Caputo–Fabrizio derivative without singular kernel to fractional Schrödinger equations.* Pramana, 2020. **94**(1): p. 92.
31. Ali, F., et al., *Flow of magnetic particles in blood with isothermal heating: A fractional model for two-phase flow.* Journal of Magnetism and Magnetic Materials, 2018. **456**: p. 413-422.
32. Ali, F., et al., *The impact of magnetohydrodynamics and heat transfer on the unsteady flow of Casson fluid in an oscillating cylinder via integral transform: A Caputo–Fabrizio fractional model.* Pramana, 2019. **93**(3): p. 47.

33. Maiti, S., S. Shaw, and G.C. Shit, *Caputo–Fabrizio fractional order model on MHD blood flow with heat and mass transfer through a porous vessel in the presence of thermal radiation.* Physica A: Statistical Mechanics and its Applications, 2020. **540**: p. 123149.
34. Jamil, D.F., et al., *Analysis of non-Newtonian magnetic Casson blood flow in an inclined stenosed artery using Caputo-Fabrizio fractional derivatives.* Computer Methods and Programs in Biomedicine, 2021. **203**: p. 106044.
35. Rajagopal, K.R., *On a hierarchy of approximate models for flows of incompressible fluids through porous solids.* Mathematical Models and Methods in Applied Sciences, 2007. **17**(02): p. 215-252.
36. Fetecau, C., C. Fetecau, and M.A. Imran, *On Stokes problem for fluids of Brinkman type.* Mathematical Reports, 2011. **13**(1): p. 15-26.
37. Saffman, P.G., *On the stability of laminar flow of a dusty gas.* Journal of fluid mechanics, 1962. **13**(1): p. 120-128.
38. Marble, F.E., *Dynamics of a gas containing small solid particles.* Proc. 5th AGARD Combustion, 1963, 1963.
39. Saffman, P., *On the stability of laminar flow of a dusty gas.* Journal of fluid mechanics, 1962. **13**(1): p. 120-128.
40. Marble, F.E., *Dynamics of a gas containing small solid particles.* Combustion and Propulsion, 1963. **5**(147): p. 175-2013.
41. Mandal, P.K., *An unsteady analysis of non-Newtonian blood flow through tapered arteries with a stenosis.* International journal of non-linear mechanics, 2005. **40**(1): p. 151-164.
42. Podlubny, I., *Fractional differential equations: an introduction to fractional derivatives, fractional differential equations, to methods of their solution and some of their applications*. 1998: elsevier.
43. Zafar, A.A., N.A. Shah, and I. Khan, *Two phase flow of blood through a circular tube with magnetic properties.* Journal of Magnetism and Magnetic Materials, 2019. **477**: p. 382-387.
44. Azhar, W.A., D. Vieru, and C. Fetecau, *Free convection flow of some fractional nanofluids over a moving vertical plate with uniform heat flux and heat source.* Physics of Fluids, 2017. **29**(8).

45. Shah, N.A., D. Vieru, and C. Fetecau, *Effects of the fractional order and magnetic field on the blood flow in cylindrical domains.* Journal of Magnetism and Magnetic Materials, 2016. **409**: p. 10-19.
46. Jan, S.A.A., et al., *Engine oil based generalized brinkman-type nano-liquid with molybdenum disulphide nanoparticles of spherical shape: Atangana-Baleanu fractional model.* Numerical Methods for Partial Differential Equations, 2018. **34**(5): p. 1472-1488.
47. Nandkeolyar, R. and M. Das, *Unsteady MHD free convection flow of a heat absorbing dusty fluid past a flat plate with ramped wall temperature.* Afrika Matematika, 2014. **25**: p. 779-798.